TECHNICAL REPORT STANDARD TITLE PAGE

1. Report No.	2. Government Accession No.	3. Recipient's Catalog No.

4. Title and Subtitle	5. Report Date
The Performance of Lapped Splices Under Rapid Loading	January 1975
	6. Performing Organization Code
7. Author(s)	8. Performing Organization Report No.
T. Rezansoff, M. P. Bufkin, J. O. Jirsa, and J. E. Breen	Research Report 154-2
9. Performing Organization Name and Address	10. Work Unit No.
Center for Highway Research The University of Texas at Austin Austin, Texas 78712	11. Contract or Grant No. Research Study 3-5-72-154
	13. Type of Report and Period Covered
12. Sponsoring Agency Name and Address	Interim
Texas Highway Department Planning & Research Division P. O. Box 5051 Austin, Texas 78763	14. Sponsoring Agency Code

15. Supplementary Notes

Work done in cooperation with the Federal Highway Administration, Department of Transportation.
Research Study Title: "Factors Affecting Splice Development Length"

16. Abstract

The impact or dynamic response and resistance of structures or structural components has been of increasing interest in recent years. The failures of lapped splices at the bases of some concrete highway support structures during the San Fernando earthquake led to questions as to the suitability and adequacy of a lapped splice subjected to fast loading rates. In addition, the damage produced by hurricanes and tornadoes surpasses earthquake damage and gives added impetus to the study of structural behavior under dynamic loads. In this investigation the behavior of lapped splices subjected to impact loading was studied. The objective was to compare the strength and behavior of splices under static and dynamic loads and to determine whether the design provisions based primarily on static tests could be relied on under dynamic loading conditions. Two series of tests were conducted. In the first series (eight beams), the specimens were subjected to impact loadings producing failure in either one cycle or in three to five cycles of incrementally increasing magnitude. In the second series (twelve beams), the specimens were subjected to either unidirectional or reversed cycles of impact loading. This investigation concentrates on explaining differences between dynamic (impact) and static behavior of splices. Analytical studies were carried out to help evaluate the experimental data. In general, the dynamic moment capacity of a splice is at least as large and usually larger than the static moment capacity. A splice length based on design specifications developed using static test results would appear to provide adequate capacity under dynamic loading conditions.

17. Key Words	18. Distribution Statement
lapped splices, rapid loading, static, dynamic, strength, behavior	

19. Security Classif. (of this report)	20. Security Classif. (of this page)	21. No. of Pages	22. Price
Unclassified	Unclassified	104	

Form DOT F 1700.7 (8-69)

THE PERFORMANCE OF LAPPED SPLICES UNDER RAPID LOADING

by

T. Rezansoff
M. P. Bufkin
J. O. Jirsa
and
J. E. Breen

Research Report No. 154-2

Research Project Number 3-5-72-154

Factors Affecting Splice Development Length

Conducted for

The Texas Highway Department

In Cooperation with the
U. S. Department of Transportation
Federal Highway Administration

by

CENTER FOR HIGHWAY RESEARCH
THE UNIVERSITY OF TEXAS AT AUSTIN

January 1975

The contents of this report reflect the views of the authors, who are responsible for the facts and the accuracy of the data presented herein. The contents do not necessarily reflect the official views or policies of the Federal Highway Administration. This report does not constitute a standard, specification, or regulation.

P R E F A C E

This report presents an investigation of the behavior of lapped splices under rapid impact loading. The objective was to compare the strength and behavior of splices under static and dynamic loads and to determine the applicability of design provisions for splices based on static test results to the strength of splices subjected to rapid loading.

This is the second report on work conducted under Project 3-5-72-154, "Factors Affecting Splice Development Length." Report 154-1 describes experimental work on the behavior of multiple lap splices in wide sections simulating retaining walls. Report 154-3F contains a reevaluation of splice and development length data aimed at producing new design recommendations. The program was sponsored by the Texas Highway Department and the Federal Highway Administration and administered by the Center for Highway Research at The University of Texas at Austin. Close liaison with the Texas Highway Department has been maintained through Mr. Wesley Pair and with the Federal Highway Administration through Mr. Jerry Bowman.

The project was under the general direction of Professor John E. Breen and the immediate supervision of Professor James O. Jirsa. The authors gratefully acknowledge the staff of the Civil Engineering Structures Research Laboratory at the Balcones Research Center of The University of Texas at Austin for their assistance in carrying out the experimental studies.

A B S T R A C T

The impact or dynamic response and resistance of structures or structural components has been of increasing interest in recent years. The failures of lapped splices at the bases of some concrete highway support structures during the San Fernando earthquake led to questions as to the suitability and adequacy of a lapped splice subjected to fast loading rates. In addition, the damage produced by hurricanes and tornadoes surpasses earthquake damage and gives added impetus to the study of structural behavior under dynamic loads.

In this investigation the behavior of lapped splices subjected to impact loading was studied. The objective was to compare the strength and behavior of splices under static and dynamic loads and to determine whether the design provisions based primarily on static tests could be relied on under dynamic loading conditions.

Two series of tests were conducted. In the first series (eight beams), the specimens were subjected to impact loadings producing failure in either one cycle or in three to five cycles of incrementally increasing magnitude. In the second series (twelve beams) the specimens were subjected to either unidirectional or reversed cycles of impact loading.

Previous studies of specimens subjected to static loads have given considerable insight into the tensile splitting mechanism occurring during failure of a splice. This investigation concentrates on explaining differences between dynamic (impact) and static behavior of splices. Analytical studies were carried out to help evaluate the experimental data.

In general, the dynamic moment capacity of a splice is at least as large and usually larger than the static moment capacity. Dynamic splice moments as large as the static capacity were safely carried for loading rates that induced steel strain rates as high as 0.3 in./in./sec. Therefore, a splice length based on design specifications developed using static test results would appear to provide adequate capacity under dynamic loading conditions.

S U M M A R Y

The objective of this investigation was to study the behavior of lapped splices subjected to impact loading and to compare the strength and behavior of splices under static and dynamic loads. The study was aimed toward determining whether design provisions based primarily on static tests could be used to design splices subjected to dynamic loading conditions.

A total of 20 specimens was tested. In the first series of tests specimens were subjected to impact loadings producing failure in either one cycle or in three to five cycles of incrementally increasing magnitude. In the second series of tests specimens were subjected to either unidirectional or reversed cycles of impact loading at a level less than that producing failure in one loading.

For dynamic loads with strain rates as investigated herein, moments acting on the splice with magnitudes equal to the static capacity can be carried over many applications of unidirectional or reversed impact loading without deterioration leading to failure. When dynamic moments exceeding the static moment capacity are applied, the maximum splice capacity is dependent on the rate of loading. The loading rate determines the dynamic yield stress of the steel and the dynamic tensile strength of the concrete.

Evaluation of dynamic splice performance included consideration of toughness and durability characteristics. The placement of stirrups along the splice greatly enhanced all toughness and durability characteristics of the splice. Dynamic loads were sustained with total deflections of at least twice the deflections found in similar specimens without splice stirrups.

In general, the dynamic moment capacity of a splice is at least as large and usually larger than the static moment capacity. Therefore, splice lengths based on design specifications developed using static test results should be adequate for splices under dynamic loading conditions.

I M P L E M E N T A T I O N

For dynamic loads with strain rates in the range considered in this study, moments acting on the splice with magnitudes equal to the static capacity can be carried over many applications of unidirectional or reversed impact loading without deterioration leading to failure. When dynamic moments exceeding the static moment capacity are applied, the maximum splice capacity is dependent on the rate of loading. The loading rate establishes the dynamic yield stress of the steel and the dynamic tensile strength of the concrete.

In general, the dynamic moment capacity of a splice is at least as large and usually larger than the static moment capacity. Dynamic splice moments as large as the static capacity were safely carried for loading rates that induced steel strain rates as high as 0.3 in./in./sec. Therefore, a splice length based on design specifications developed using static test results would appear to provide adequate capacity under dynamic loading conditions.

TABLE OF CONTENTS

L I S T O F T A B L E S

L I S T O F F I G U R E S

N O T A T I O N

b = Width of beam

E = Modulus of elasticity

f'_c = Compressive strength of concrete

f_s = Steel stress

f_y = Yield strength of reinforcement

FMAX = Maximum force level reached by forcing function

F(t) = Force applied to beam, varies with time

I = moment of inertia

L = Beam length

L_s = Splice length

M = Moment along splice

MR = Moment along splice determined from measured reaction

M_ϵ = Moment along splice determined from measured strain

M_D = Moment capacity of beam tested under dynamic loads

M_s = Moment capacity of beam tested under static loads

M_y = Moment capacity at yield in reinforcement

T = Fundamental natural period

TC = Time when force remains constant

TD = Time for force to decline

TR = Rise time

TS = Starting time for forcing function

W = Circular frequency

Δ = Beam deflection

ΔMAX = Maximum beam deflection

ϵ_c = Strain at center of splice

ϵ_E = Strain at end of splice

ϵ_{yD} = Dynamic yield strain of reinforcement

μ = Unit length mass density

CHAPTER 1

INTRODUCTION

1.1 Background

To maintain continuity in concrete construction and to meet limitations imposed by bar lengths and fabrication or placement requirements, some form of connection between reinforcing bars is needed in most structures. Lapped splices are often the simplest, most economical connection between two bars. The mechanism of load transfer between lapped deformed bars is dependent on the tensile strength of the concrete and on the cover thickness. The cover tends to split away from the bar due to force components normal to the bar axes. Additional resistance can be provided by transverse reinforcement or other confinement provided to control splitting. The load transfer provided by adhesive or cohesive "bond" resistance is minimal compared with that provided by interlock between the bar deformations and the concrete. However, the term "bond stress" is widely accepted.

The investigation detailed herein represents one stage of a long-range study at The University of Texas at Austin into the behavior of lapped splices. Variables that have been or are currently being studied in connection with lap splices include lap length, bar size, steel strength, bar spacing, concrete cover, moment gradient, stirrup or other form of concrete confinement and the rate of loading. Specialized splices such as welding and positive mechanical connections have also received attention.

The impact or dynamic response and resistance of structures or structural components has been of increasing interest in recent years. Ground motions measured during the San Fernando earthquake [1] were more severe than previously considered possible and have resulted in a tightening of design provisions in seismic zones. The failures of

lapped splices at the bases of some concrete highway support structures during the San Fernando earthquake lead to questions as to the suitability and adequacy of a lapped splice subjected to fast loading rates. In addition, the yearly devastation produced by hurricanes and tornadoes, which cumulatively far surpasses earthquake damage, gives impetus to the study of structural behavior under dynamic loads. Vehicular impact may also produce loading rates exceeding those normally considered in design.

1.2 Object and Scope

In this investigation the behavior of lapped splices subjected to impact loading was studied. The objective was to compare the strength and behavior of splices under static and dynamic loads and to determine whether the design provisions based primarily on static tests could be relied on under dynamic loading conditions.

Two series of tests were conducted. In the first series, eight beams were tested to determine the influence of lap length on the strength and response of the beam [2]. The specimens were subjected to impact loadings producing failure in either one cycle or in three to five cycles of incrementally increasing magnitude. The second series of tests included twelve beams. Four specimens contained 18 in. splices. Three were subjected to unidirectional cyclic impact loading. One was subjected to static loading. Eight beams had 30 in. splices and were subjected to either unidirectional or reversed cycles of impact loading. Load cycles were applied at a level less than that producing failure in one loading to destruction of the splice. The results of four beams with lap splices, tested statically in a previous study [3], are used as a reference for static behavior.

Previous studies of specimens subjected to static loads have given considerable insight into the tensile splitting mechanism occurring during failure of a splice. This investigation concentrates on explaining differences between dynamic (impact) and static behavior of splices. The variation occurring in the material properties of steel and concrete subjected to different rates of loading is examined. The beam cross

section and area of tensile reinforcing steel in the splice were the same throughout. Two point symmetrical loading was applied to the simply supported beams to achieve a condition of constant moment and zero shear over the splice lap length. Analytical studies were carried out to help evaluate the experimental data and explain the higher mode response measured in the tests.

CHAPTER 2

EXPERIMENTAL PROGRAM

The test program was established to compare the behavior of lapped splices under impact loading to similar splices tested statically. The following criteria were considered in the selection of the test specimens. The specimens were proportioned to ensure splice failure rather than shear or flexural failure. To eliminate the effect of shear and moment gradient over the splice region, a two point symmetrical loading system was designed to produce a constant moment over the splice length.

2.1 Specimen Details, Notation and Loading

The specimens duplicated the beam dimensions, tension reinforcement and splice details of beams tested previously under static loads. The prime variables include type of loading applied, splice length, and amount of transverse reinforcement in the splice region. Details of the test specimens are shown in Fig. 2.1 and Table 2.1.

Reference Static Tests (Series SR). Four beams statically tested by Ferguson and Breen [3] were selected as a reference for evaluation of dynamic behavior. The basic cross section was 17 × 15 in. with two #8 bars and is identical to the first cross section illustrated in Fig. 2.1(a), except for the omission of the two #4 top bars. Test results for lap lengths of 18 in., 30 in. and 42 in. were available from this study. One beam of each lap length contained no stirrups in the splice region while the fourth beam had a 30 in. lap length and #2 stirrups at 4.5 in. over the splice. Longitudinal details and stirrup reinforcing for the various lap lengths are contained in Fig. 2.1. The reference static tests (RS) are denoted as 8R18a, 8F30a, 8F30b, and 8F42a in the original report. The notation 18, 30 and 42 refers to the lap splice length in inches, while the "b" designates the stirrups in the splice region.

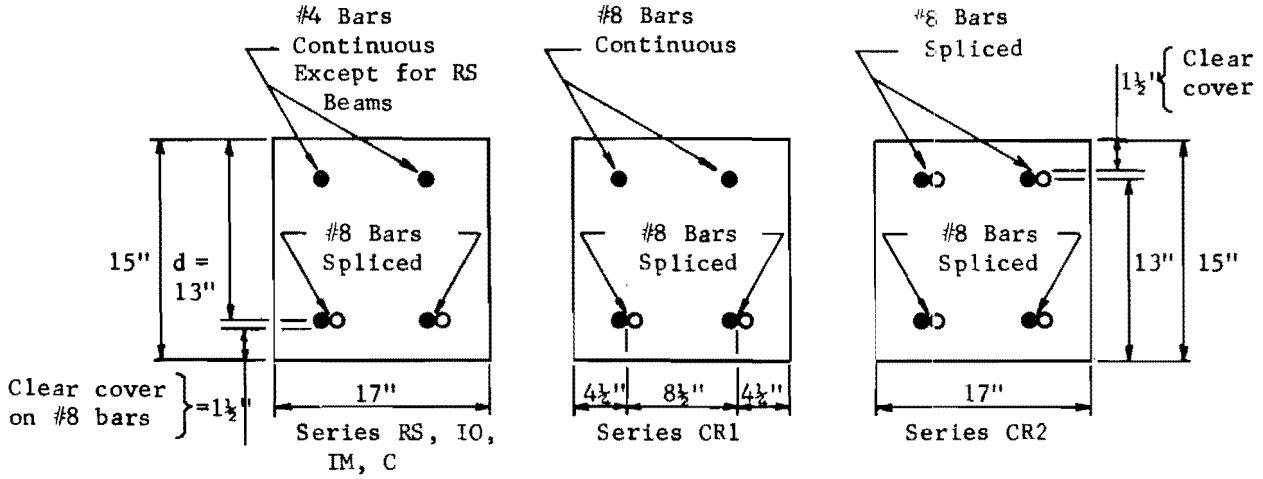

(a) Beam cross sections

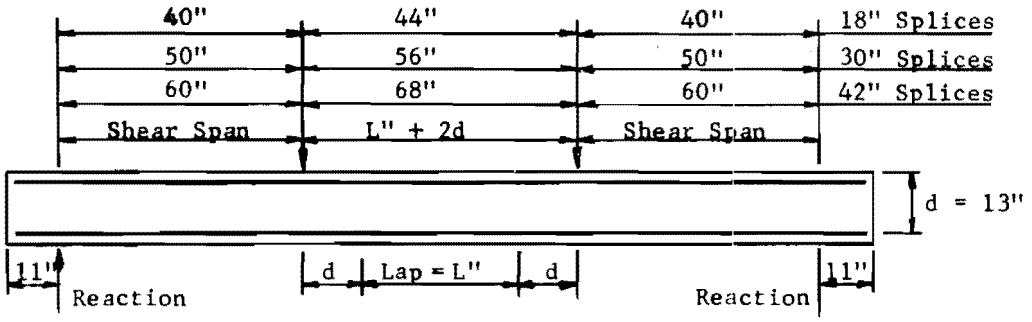

(b) Longitudinal details - side view

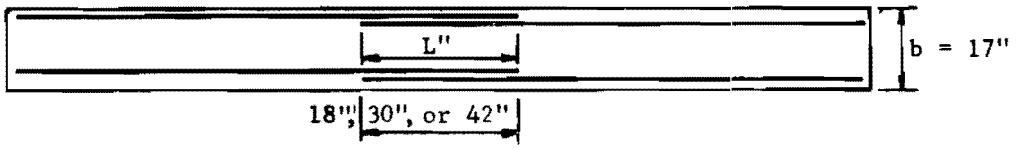

(c) Splice lay out - plan view

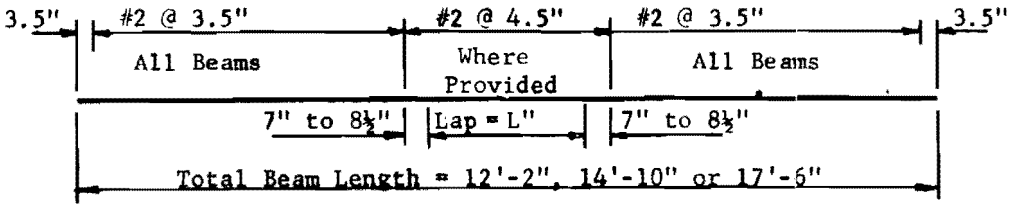

(d) Stirrup reinforcing

Fig 2.1. Specimen details

TABLE 2.1. DETAILS OF TEST SPECIMENS

Series	Splice Length in.*	Transverse Reinforcement*	f'_c psi	Age at Testing Days	Notes
RS	18		3470		Reference Static Tests
RS	30		3030		(From Ref. 3)
RS	30	T	2610		
RS	42		2660		
IM	18		3180	43	Incremental Loading
IO	18		3180	47	(Impact)
IM	30		3160	43	(O - one loading to
IO	30		3160	43	failure)
IM	30	T	3610	28	(M - multiple loads
IO	30	T	3610	29	increasing incre-
IM	42		3260	21	mentally)
IO	42		3260	21	
C	18-S		3330	95	Cyclic Loads (Impact)
C	18-1		3330	100	(C - repeated loading)
C	18-2		3400	30	(CR1 - reversed load-
C	18-3		3400	31	splice one face
C	30-1		4060	68	only)
C	30-2		4060	69	(CR2 - reversed load-
C	30-1	T	3820	64	splice both faces)
C	30-2	T	3820	67	
CR1	30		4320	88	
CR2	30		4320	95	
CR1	30	T	3340	56	
CR2	30	T	3340	57	

*Notation following splice length indicates several tests with same details, S is static test for reference in C series.

**T denotes transverse reinforcement in splice region, #2 @ 4.5 in.

Incrementally Increasing and Single Impact Tests (Series IO, IM). Four pairs of beams were tested with each pair duplicating the lap lengths and stirrups of the reference static beams. One beam of each pair was subjected to a series of three to five cycles of increasing load until failure was reached (Series IM). Failure was categorized by either a total collapse of the specimen resulting from separation of the lap splice (splice failure), or large deformation of the specimen with substantial yielding of the tensile reinforcing steel (flexural failure) without a splice failure. The flexural failure mode was observed for the 42 in. splice (Specimen IM-42) and the 30 in. splice with stirrups through the splice region (IM-30T).

The second beam of each pair was subjected to a single impact load to failure (Series IO). The magnitude of load required to produce failure in one load application was estimated on the basis of results of the incrementally increasing load test. Since each pair of beams was cast from the same batch, concrete strength was not a variable for any given pair. Failures similar to those in the IM series were observed.

Cyclic Loading (C, CR Series). Four beams with 18 in. splices were investigated to examine the ability of a lap splice to sustain a specified load level under repeated impact loading. All four beams were identical and did not have stirrups along the splice length. One beam (C-18-S) was tested statically as a control beam and provided a check on the data of reference static test (RS-18). The remaining three beams (C-18-1,2,3) were tested under repeated impact loads. The loading was regulated so that the maximum moment occurring along the splice would be greater than the failure moment under static loading and less than the failure moment obtained under incrementally increasing loads or single loading to failure. The number of load cycles required to produce failure at a particular load level gave a qualitative evaluation of the splice performance.

The 18 in. splices demonstrated the effect of dynamic load repetitions because of the very large difference in capacity between static and incrementally increasing or single impact loading. However,

an 18 in. tension lap splice for a #8 bar is about one-third the length of 51-1/2 in. proposed by Ferguson and Krishnaswamy [3] for Grade 60 bars, f'_c = 3000 psi and spacing and concrete cover as in the specimens. ACI [4] or AASHTO [11] specifications require a length of 47.1 in. for a Class C splice (all bars spliced, stress $> 0.5f_y$). Since the 42 in. splices failed in flexure in Series IO and IM, splice lengths of 30 in. were selected for the remaining tests. Four were designated for repeated cyclic loading (Series C); two with and two without stirrups over the lap splice. Initially one beam of each pair was to reach failure under a single impact load. However, the loading energy levels (mass drop heights) chosen underestimated the beam strengths and did not produce failure under one load application. As a result, these beams were subjected to repeated loading at very high load levels, while the companion beams were tested under repeated low load levels.

Four specimens with 30 in. splices were subjected to cyclic reversals (Series CR) to study the influence of alternating cycles of tension and compression loading on the splice. Slip between the splice bars and the concrete occurring during a tensile load would tend to be reversed upon application of a compression load with a resulting deterioration of the stress transfer capability between steel and concrete. Tension steel was required in both faces for the CR Series. Two of the four beams subjected to load reversal had splices only in the bottom layer of steel with continuous bars in the top layer (CR1-30, CR1-30T). Specimens CR2-30 and CR2-30T had identical splices in both the top and bottom faces. The beams with splices on both faces gave an indication of the influence of top casting on splice performance.

2.2 Materials

The material properties were obtained under static or low strain rates. The change in properties resulting from the very high strain rates applied in the dynamic tests are considered in Chapter 5.

Concrete. The concrete strengths and age at testing for the impact specimens are tabulated in Table 2.1. Specimens cast in pairs are shown to have the same concrete strength, even though the age at

testing may have varied by as much as a week. The specimens tested at the largest age difference had been cured under atmospheric conditions for some three momths, so an age differential of five to seven days did not significantly affect concrete strength. Four 6 X 12 in. control cylinders were cast with each specimen. The strength range for all specimens and the static reference beams varied from 2610 psi to 4320 psi.

Concrete for all test specimens was obtained from a commercial ready-mix supplier. Concrete for beams subjected to single or incrementally increasing loads was proportioned to obtain strengths similar to those of the reference static tests. The following mix proportions and properties were selected:

Water/cement ratio:	5.84 gal./sack (0.52 lb./lb.)	% of total by weight
Cement content:	4.4 sacks/yd.^{3}	10.0
Water content:		5.2
Coarse aggregate	5/8 in. max. Colorado River Gravel	51.2
Fine aggregate		33.6
		100.0
Slump:	3 - 6 in.	
Admixtures:	Airsene, a cement dispersing admixture (1 oz./22 lb. of cement)	

The concrete mix portions used for the specimens under repeated loads were slightly modified. Mix proportions and properties were as follows:

Water/cement ratio:	7.33 gal./ sack (0.65 lb./lb.)	% of total by weight
Cement content:	4.26 sacks/yd.^{3}	10.0
Water content:		6.5
Coarse aggregate:	1 in. max.	44.4
Fine aggregate:		39.1
		100.0
Slump:	2 - 4 in.	
Admixtures:	None	

The specified mix designs were not strictly maintained by the concrete supplier, leading to some scatter in the resulting concrete strengths. The time intervals between some of the castings resulted in variations in the type and moisture content of the aggregate. In some instances additional water was added to the concrete before casting to increase slump and workability. The large age differences at testing for the various batches influenced concrete strengths even if the mix proportions were identical. Specimens could not be tested at a specified age because instrumentation needed for the study was in use on other projects and could not be precisely scheduled for use.

Specimens were cast in steel forms and control cylinders were cast in steel molds. Mechanical vibrators were used to ensure good concrete compaction around the reinforcing steel. Mechanical vibrators were also used to compact the concrete cylinders. Specimens and cylinders were cured in the forms for several days with moist quilting or polyurethane sheets used to prevent rapid water loss from exposed surfaces. After removal from the forms, the specimens were cured in the laboratory until testing.

Reinforcing Steel. Tension reinforcement in all specimens consisted of #8 bars of Grade 60 steel. For the C and CR series the average yield strength at a strain offset of 0.2 percent for three representative tension tests was 60 ksi. The yield strength for the IO and IM series was 63.3 ksi. Transverse reinforcement was fabricated from 1/4 in. plain bars, with a yield stress of about 50 ksi.

The reference static tests contained steel with yield strengths varying between 64 ksi and 100 ksi. However, all failures occurred prior to the steel yielding, thereby eliminating the influence of variable yield strengths.

2.3 The Loading System

The system was designed to provide forces with variable peak levels for testing various lap length and stirrup arrangements used in the specimens, under both incrementally increasing and single impact load applications. To obtain load rates more typical of seismic or

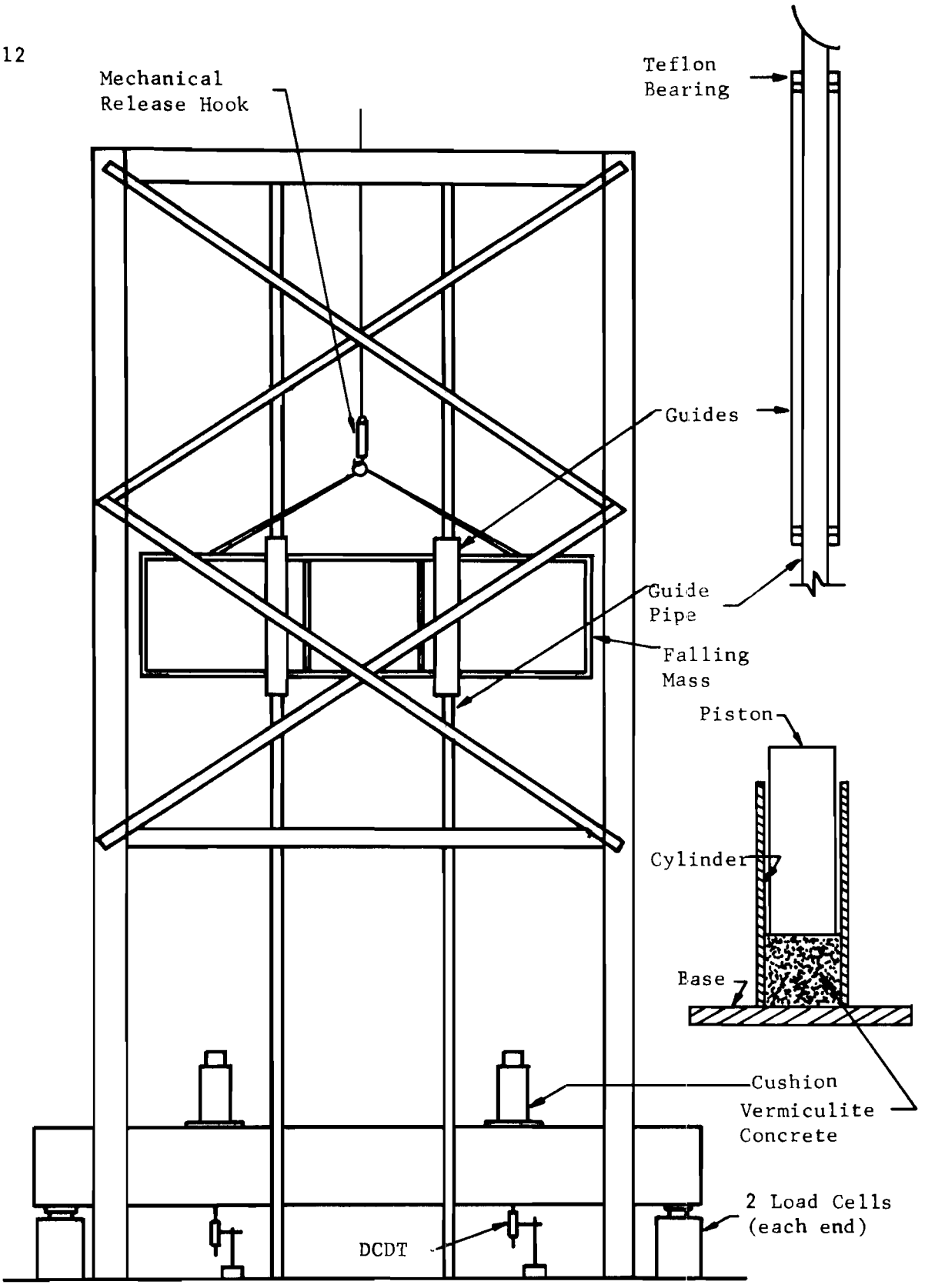

Fig. 2.2. Schematic of dynamic loading system

wind loading, it was necessary to alter the load pulse typical of an impact loading. By cushioning the impact, forces approximated a bilinear ramp with load maintained over a sufficient time to allow for maximum bending of an elastic specimen under the applied load level. Finally, a constant moment region over the splice was needed to eliminate the effects of shear on splice performance.

Drop Mass and Guide System. The loading system is illustrated by the schematic in Fig. 2.2 and the photograph in Fig. 2.3. The main feature of the system was a falling mass which impacted the specimen through cushioning devices. The mass was raised to the chosen drop height using an overhead crane and a quick release hook (used for helicopter drop applications) was manually released.

The drop mass was fabricated using three 8 ft. lengths of W24X76 steel sections placed side by side with flange tips welded together. Half inch plate stiffeners were welded across both ends and across the third points of the outer halves of the two outside wide flange members. Three 7 in. wide by 27 in. long channels running laterally across the top of the three wide flange shapes were attached with legs outstanding to provide lateral continuity. A 1 in. plate was welded to the bottom flanges to provide further continuity and ensure a smooth impact surface. Four bent bars were welded to the top face channels to provide loops for connecting turnbuckle bolts to the quick release hook. The turnbuckles permitted leveling of the drop mass to ensure near simultaneous impact of the mass on the two cushioning devices. The total mass weight was 2600 lbs. and the moment of inertia of the combined three wide flange sections and the bottom steel plate was 8500 $in.^4$.

Four 2 in. diameter steel pipes were used to guide the falling mass. The pipes were attached to the test floor and the top of a 20 ft. high braced steel frame and tensioned to improve the lateral stiffness of the pipes and the alignment of the falling mass. Two 26 in. long, 3 in. diameter steel pipes with greased, teflon bearings were attached to each side of the drop mass and traveled over the tensioned pipe guides.

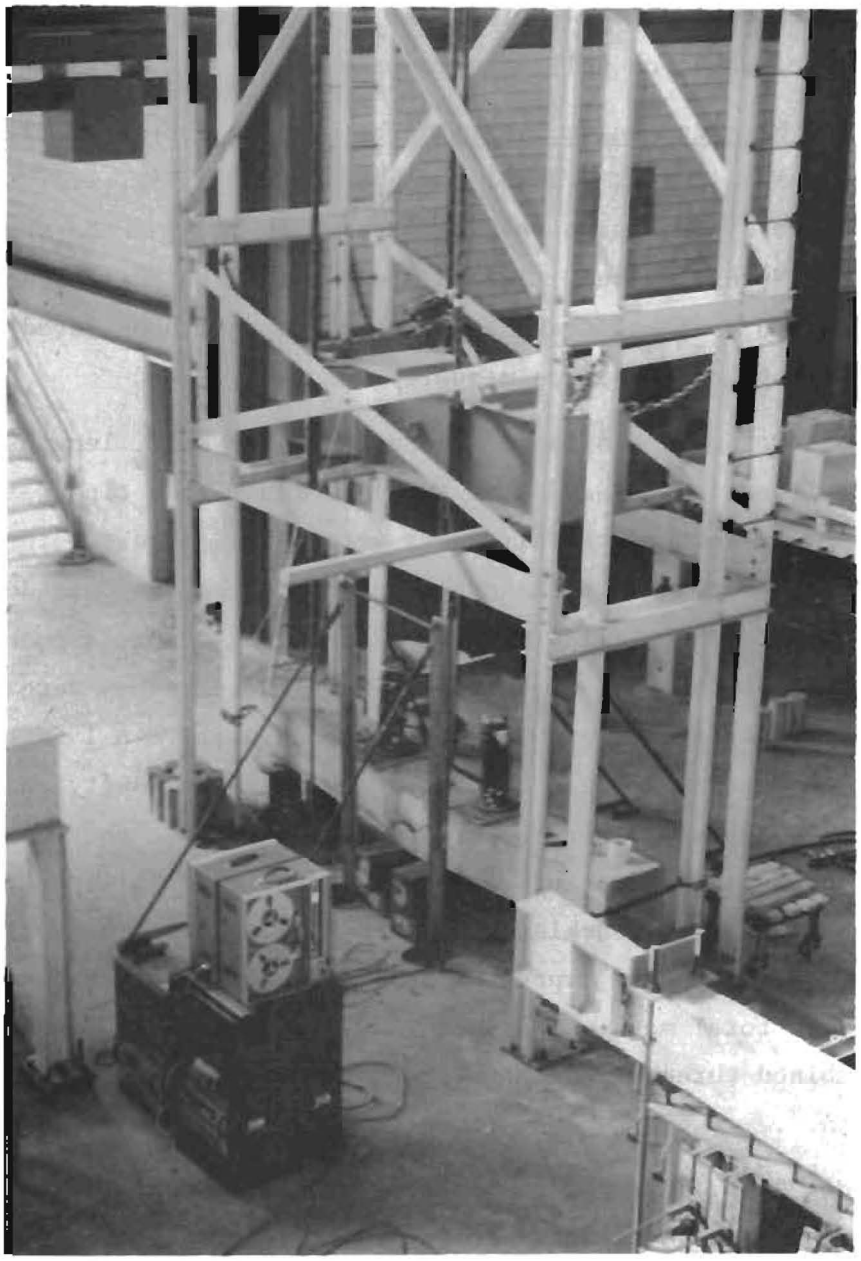

Fig. 2.3 Dynamic Loading System.

The guide system provided a total of eight teflon bearings for maintaining the lateral and rotational positioning of the drop mass.

Cushioning Devices. Cushioning devices were used to provide an acceptable force-time relationship for the load pulses. The schematic of Fig. 2.2 illustrates the component parts of the cushioning devices. Six in. diameter vermiculite concrete cylinders were placed in 6.2 in. inside diameter steel cylinders with closed bases that rested on the test specimen at the load points. Steel pistons which extended above the steel confining cylinders and rested on the vermiculite cushions received the direct impact of the falling mass. Compression of the vermiculite concrete between the specimen and the drop mass increased the rise time, reduced the peak force magnitude and extended the pulse time of the impact load on the specimen. Removable bases on the steel confining cylinders facilitated removal of the compressed vermiculite after loading.

For the specimens subjected to increasing incremental and single impact loads various combinations of the height of the vermiculite cylinders and diameters of the steel pistons were used. Attempts were made to achieve specific load levels with desirable load-time characteristics by using 4 in. to 8 in. heights of vermiculite cylinders, 3 in., 4 in., or 6 in. diameter steel pistons and various drop heights.

Vermiculite Concrete. The use of vermiculite concrete as a cushioning material was studied previously and reported in Refs. [4] and [5]. Mix properties and a casting procedure were chosen to produce a vermiculite concrete similar to one documented by Smith and Thompson[4]. Two different vermiculite aggregates were used because the one used initially became unavailable as the study progressed. As a result the water content was altered slightly to maintain approximately the same slump with both aggregates. The concrete consistency and workability were very dependent on the water content used with a particular aggregate. Some experimentation was necessary to determine optimum proportions. Mix proportions for casting 11 to 12 standard 6X12 in. cylinders are presented in Table 2.2. Properties of the vermiculite concrete are also shown.

TABLE 2.2. VERMICULITE CONCRETE PROPORTIONS AND PROPERTIES

Vermiculite Type	Zonolite Plaster Aggregate Type FR		Zonolite Concrete Aggregate ASTM Spec. C-332-66 Group 1	
	Series IO, IM	Series C-18	Series C-30	Series CR
Vermiculite Weight per Batch	21.0 lb.	12.4%	21.0 lb.	12.7%
Cement Weight per Batch (Normal Type 1)	70.5 lb.	41.7%	70.5 lb.	42.6%
Water Weight per Batch	77.5 lb.	45.9%	74.0 lb.	44.7%
TOTAL	169.0 lb.	100.0%	165.0 lb.	100.0%
Septair (Air Entraining Agent)	110 ml.		110 ml.	
Unit Weight	54-58 lb./ft^3 (wet)		55-59 lb./ft^3 (cured)	
Slump	8 - 9-1/2"		8-1/2 - 10"	
Measured Air Content (Teckote White Air Meter)	34 - 38%		30 - 35%	
Curing	sealed individual plastic bags stored at 70°F for a minimum of 28 days before use.		polyurethene sheet covering around entire perimeter of the stacked cylinders stored at 70°F for a minimum of 28 days before use.	

The energy absorbing characteristics of the vermiculite concrete are highly dependent on the air content. To obtain a uniform product, the mixing and casting techniques had to be standardized. An improper sequence for combining the components of the concrete in the mixer resulted in a homogeneous mix. Excessive mixing time reduced the desired air content. The procedure followed one outlined in Ref. [4]. Using a Muller rotary drum mixer with a capacity of 3 $ft.^3$ the following procedure proved satisfactory.

1. The air entraining admixture (Septair) and water were combined and stirred thoroughly in a separate container.
2. Approximately 40 percent of the water was placed in the mixer. All the vermiculite aggregate was added in three stages with the mixer rotated one third of a revolution for each stage. The aggregate and water was mixed for 1-1/2 minutes.
3. All the cement was placed in the mixer in three stages and mixed for a total of 1-1/2 minutes. During the mixing stage, the mixer was stopped once to manually stir cement at the bottom of the mixer which was not combining with the aggregate-water mixture.
4. The remaining 60 percent of the water was added to the mixer while it slowly rotated. The mixer was run for a total of five minutes, stopping once or twice to check that the mix was combining uniformly.
5. Air content and slump tests were performed and the steel cylinder molds were cast. Instead of rodding, the containers were tapped sharply ten times for each one third volume of concrete placed.

2.4 Instrumentation and Data Recording

Signals for the reactions, steel strains and the load point deflections were recorded on magnetic tape to give a continuous time history of the response for every load application. The rapid loading rate required the use of high speed tape recorders operating at 30 in. per

second to record the data with sufficient resolution. Two 8-track FM tape recorders were used.

A system of signal conditioners and amplifiers were used to modify voltages from strain gages, reaction load cells and displacement transducers to produce signals compatible with the tape recorder input. For evaluation, the raw data contained on the magnetic tape were reproduced using a light beam oscillograph. A schematic of the data recording and reproduction system is provided in Fig. 2.4.

One channel of each magnetic tape record was used to establish a common time reference signal, so that all data from both tapes could be referenced to the same instant in time. Four of the channels were used for recording reactions and deflections. Remaining channels were used to obtain a representative sampling of reinforcing steel strains in the splice region.

Reactions and Deflections. Reactions were measured by two pairs of load cells with 100,000 lb. capacity. Connection of two load cells in parallel resulted in a single data signal for each reaction. Deflections at the load points were measured with direct current deformation transducers with a range of travel of ± 3 in.

Reinforcing Steel Strains. Strains were measured with electrical resistance strain gages bonded to the bars. After grinding the bar deformations and filing mill scale at the gage location the surface was prepared using a metal conditioner and cleaner. The gages were attached with either contact or epoxy cement. The gages were waterproofed prior to casting. Strain gages were generally located at the start of the splice and at the midlength.

2.5 Test Procedures

After each loading, cracks were marked and labeled. The extent and patterns of these cracks gave qualitative information on the performance of the specimen under impact. Longitudinal cracking on the tension face directly below the spliced bars indicated splitting along the splice which led to deterioration of the splice. Figures 2.5 and 2.6 show crack

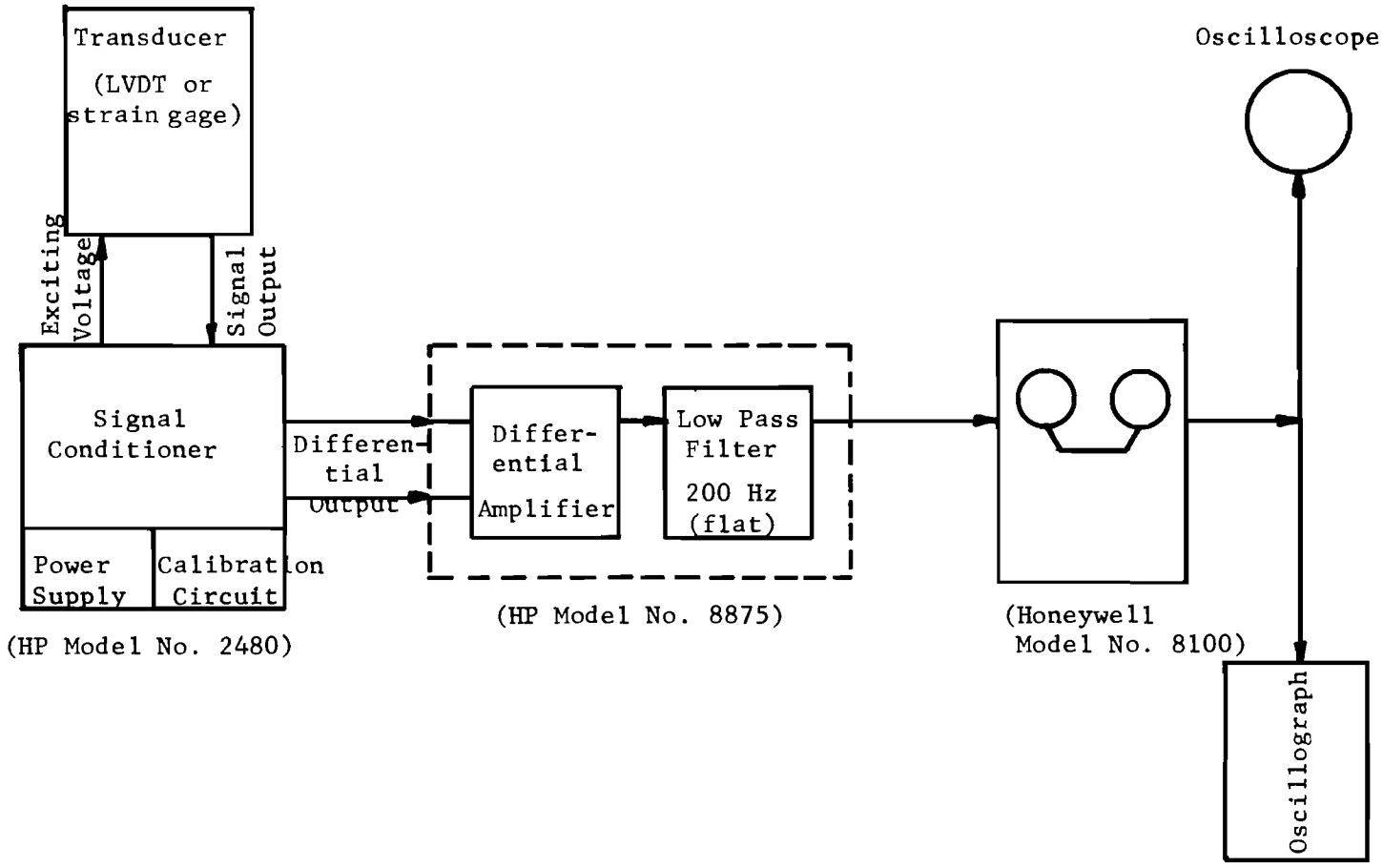

Fig. 2.4. Data recording and reproduction system

Fig. 2.5. Specimen C-18-2 after failure

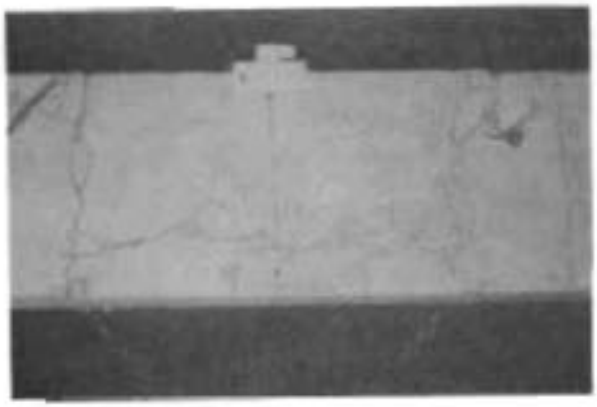

Top Splice

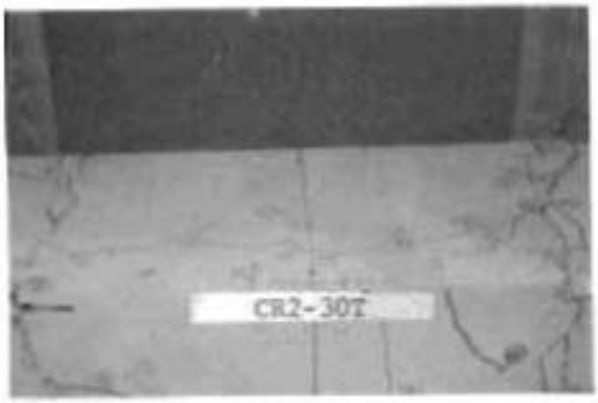

Top Corner View

Side View

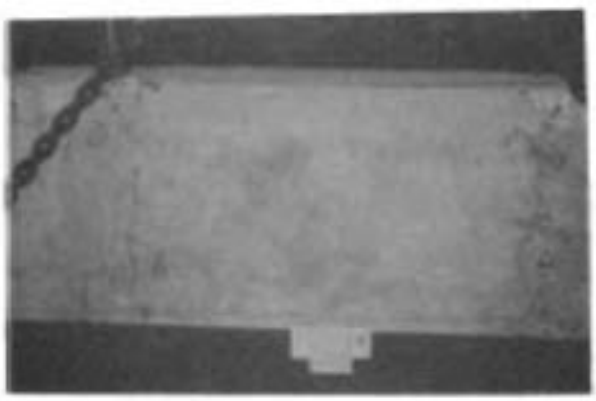

Bottom Splice

Fig. 2,6. Specimen CR2-30T after failure

patterns for two specimens. The large shear crack in Fig. 2.5 was the result of deformations following splice failure. Figure 2.6 shows the wide flexural crack at the ends of the splice and the longitudinal splitting crack along the top bars which led to failure.

Dial indicators were used on some specimens to record the residual deflection history at the beam load points. This duplication served not only as a check on the residual deflections recorded by the DCDT's, but also indicated the extent of inelastic behavior occurring while testing was in progress. Since the magnetic tape data of the DCDT's could not be conveniently monitored during testing, the dial gages gave a simple method of recording the total residual deformation present and the residual deflection increment produced by one impact. Adjustments to the load energy level (mass drop height) in some repeated loading tests were made if it became apparent that little or no residual deflection was induced after a series of equal impact loads.

The amount of energy imparted to the specimens by the drop mass depended primarily on the kinetic energy of the drop mass at impact (determined from the drop height) and the energy absorbed in compressing the vermiculite concrete cushions. Reference [4] gives an energy absorption rate of approximately 24 ft.-lb./in.^{3} for a 40 percent deformation in a vermiculite concrete of proportions similar to those used here. Attempts at predicting the force applied to the specimen by the drop mass required the determination of energy absorbed by vermiculite cushions. The protrusions of the steel pistons resting on the vermiculite prior to and just after impact were recorded to obtain the percentage deformation.

2.6 Typical Test Data

A large volume of experimental data was recorded on magnetic tape. For each loading cycle up to fourteen channels of data were recorded. A total of 19 specimens was tested with three of these specimens subjected to between 20 to 30 impact loadings and the remainder to a smaller number of loadings.

Data on the magnetic tape were reproduced onto paper traces. A representative number of data traces is presented to illustrate important features and to outline the procedures used in analyzing the data. Key features are tabulated to provide an indication of the dynamic response.

Reactions. Typical reaction-time plots are shown in Fig. 2.7. The time axis is represented on the abscissa, with reaction magnitudes measured vertically from the base line established before loading is applied. The scales for determining reaction magnitudes were established by calibrating each channel prior to initial loading. Ordinarily, the scales for the two reactions are different, so a direct visual comparison of magnitudes cannot be made and, in addition, calibrations change from specimen to specimen.

Examination of the reaction responses shows appreciable shape variations between specimens, load cycles of the same specimen, and reactions for a particular load cycle.

The measured reaction responses show that there is little consistency to the higher modes of vibration that are recorded. Some have fairly regular, easily discernible, sinusoidally varying characteristics as shown by the east reaction for Specimen CR1-30, load cycle 7. The corresponding west reaction shows the higher mode response suppressed very rapidly. For load cycle 8 of Specimen CR1-30, the higher vibration modes were not discernible. Load cycles 7 and 8 represent data from consecutive load cycles with equal drop heights of low magnitude. The reinforcing steel did not yield in these two cycles. Load cycle 4 of Specimen IM-42 is also shown in Fig. 2.7. The beam contained a 42 in. splice and the loading was sufficient to produce steel stresses well above the static yield point.

Deflections. Unlike the reactions, deflection curves were smooth and did not exhibit higher mode vibrations as can be seen in Fig. 2.8. Deflections were calibrated prior to initial loading and magnitudes determined from a base line corresponding to the trace locations prior to loading.

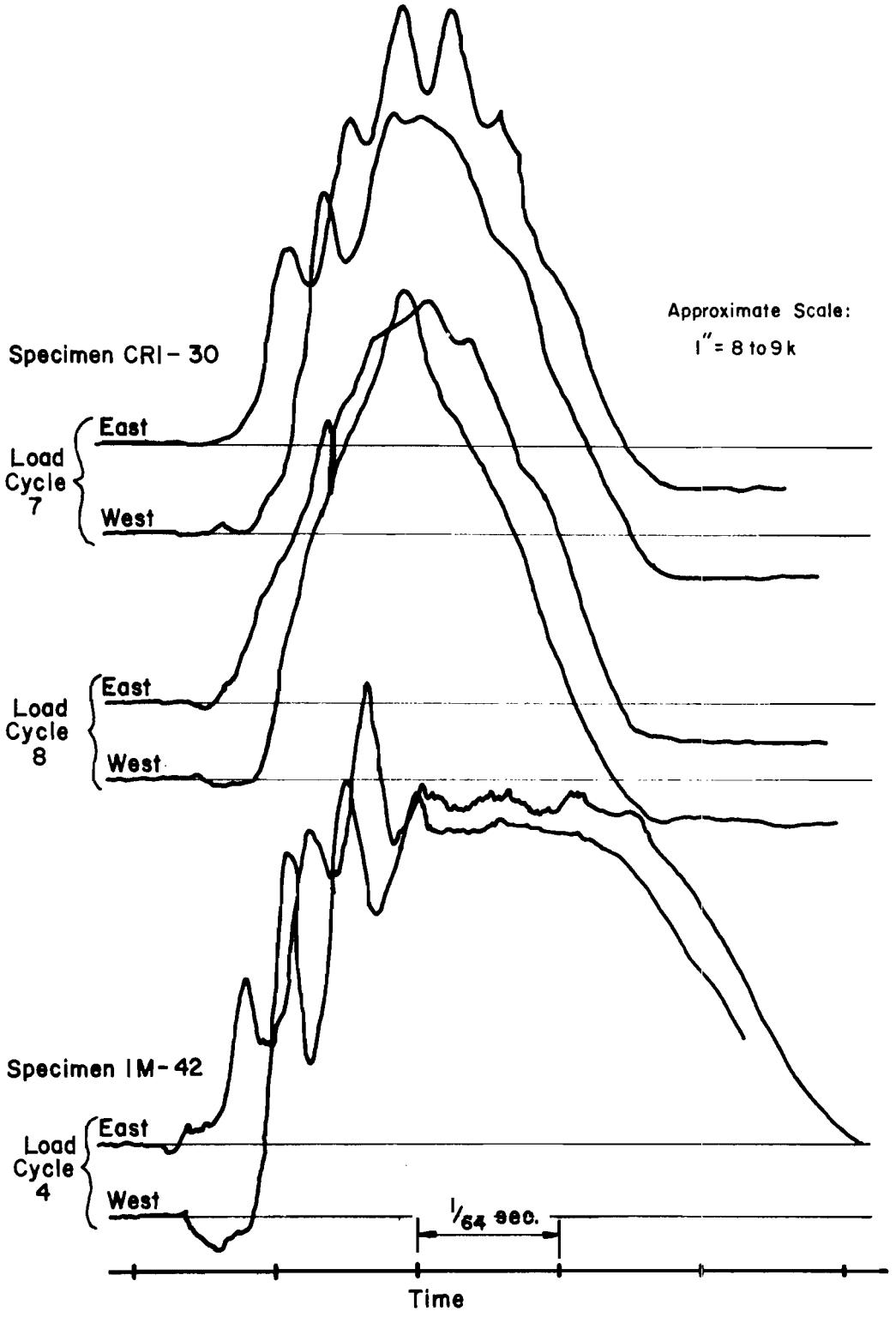

Fig. 2.7. Typical reaction data

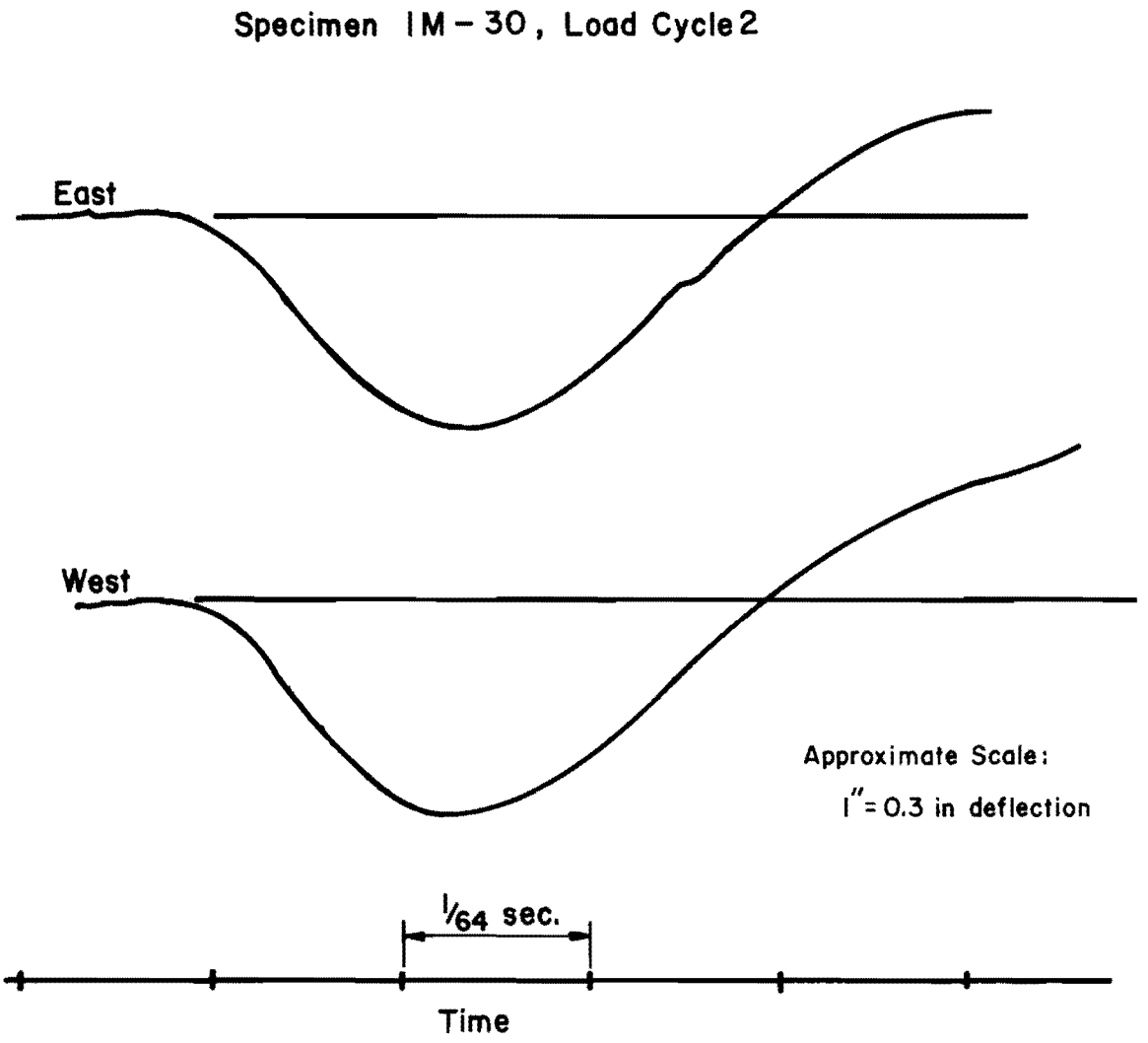

Fig. 2.8. Typical deflection data

Strains. Although reinforcing steel strains do not exhibit to a great extent the higher modes of vibration, as can be seen in Fig. 2.9, the data are often difficult to analyze. The difficulty lies in determining the time and stress level at which the reinforcing steel yields. Once the bar yields, stresses in the bars cannot be obtained from strains. The strain-time plots for Specimen CR1-30 shown in Fig. 2.9 are typical of loading levels in which yield of the reinforcing steel was not reached. The strain-time plots in Fig. 2.9 for Specimen C-30-2T show a case where reinforcing steel has yielded.

Time Reference and Scale. Because each measured response was traced from the magnetic tape onto individual plots, it was necessary to establish a common time axis reference for all data recorded during a given loading cycle. This was achieved by simultaneously tracing a common time signal on each data trace. The time reference allows the magnitudes of recorded responses to be established at any time during the test for use in detailed analyses.

In most cases the oscillograph traces reproduced from the magnetic tape were to a time scale of 15.625 milliseconds per inch of travel (effective trace speed = 64 in./sec.). In addition, some traces were reproduced with slower speeds to give a condensed time representation of the loading cycle.

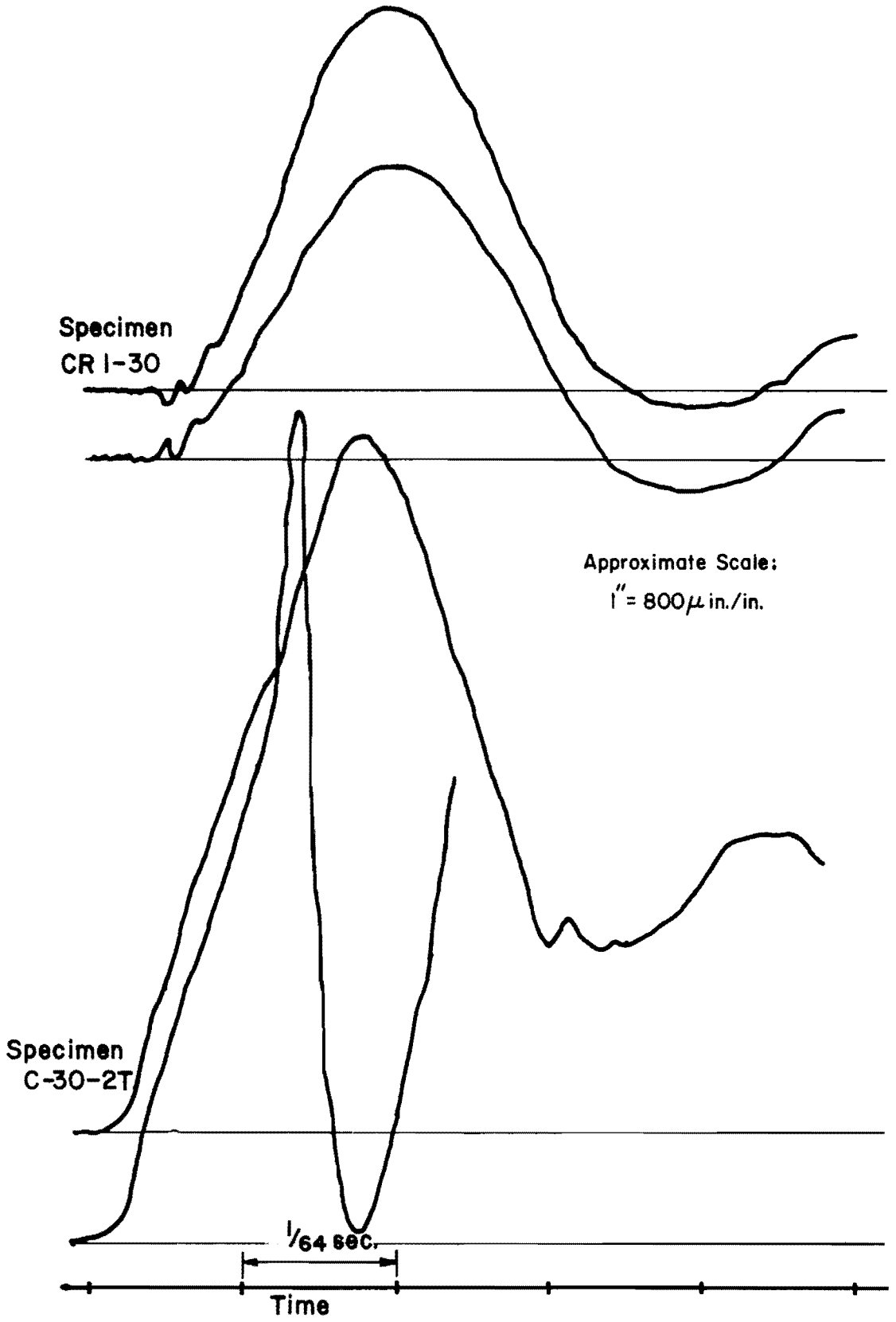

Fig. 2.9. Typical strain data

CHAPTER 3

THEORETICAL ANALYSIS OF AN ELASTIC MODEL

3.1 Introduction

A theoretical study was undertaken to determine if the measured dynamic response could be reasonably simulated analytically. The model of the concrete beam was assumed to behave elastically. The analysis was carried out using a finite (central) difference time marching algorithm for an undamped multi-degree of freedom lumped mass system. The time range over which the dynamic behavior was investigated was generally less than one period of the natural vibration of the first (fundamental) mode, and long time effects of damping were of no concern. The rotational inertia effects neglected by a lumped mass representation were of no consequence when short beam segments were used to discretize the model.

The finite difference algorithm was used to calculate directly the linear displacements of all nodes at discrete intervals of time. The variation of the displacements with time was used to obtain linear accelerations and inertial forces for the lumped masses from which reaction versus time relationships can be determined. For beam moments the rate of change of node displacements (beam deflection) along the length of the beam was used to calculate curvatures. Both acceleration and curvature were derived using the central finite difference method.

A model beam showing the nodes and degrees of freedom is illustrated in Fig. 3.1. For simplification, points of zero displacement (at the reactions) were not treated as nodes. The application of finite difference theory to obtain the solution algorithm is based on the central finite difference module for second derivatives. A three point equation is utilized. The basic module and a reference sketch are outlined in Fig. 3.2 for acceleration.

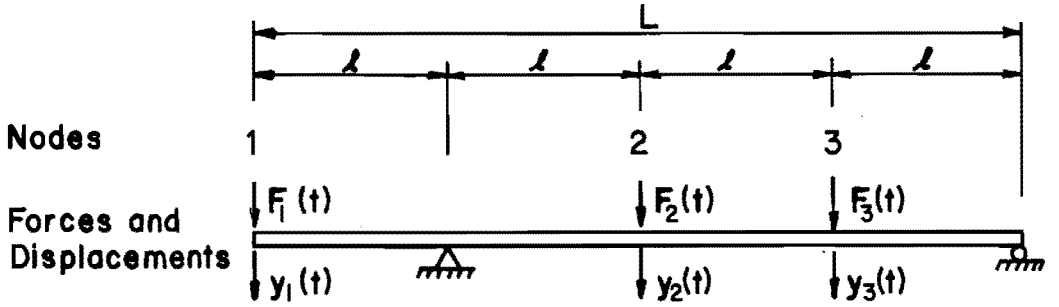

Fig. 3.1. Final discretized form for sample elastic model (overhang on one end for illustrative purposes only)

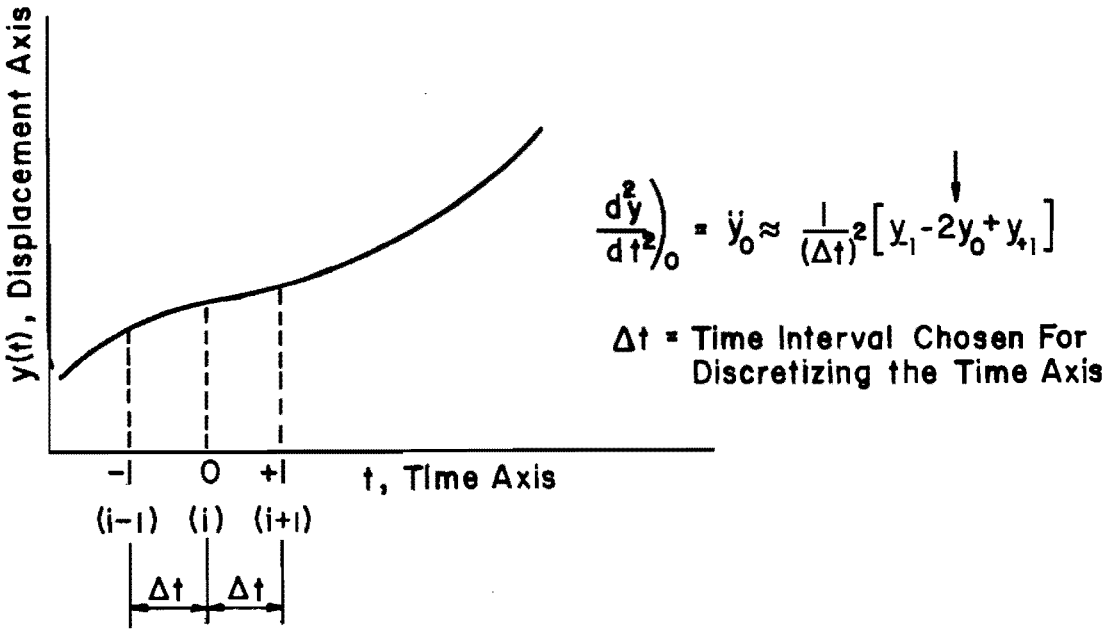

Fig. 3.2. Finite difference approximation for acceleration

Once displacements at all the nodes for the discrete time positions over the time interval being studied were calculated, the displacements were used to obtain variations in reactions and moments at the node location with time. The computer program written to solve the dynamic response of the elastic beam model is described in detail in Ref. [12]. Extensive checks were made to assure the reliability of the mathematical model used in the analysis. Solutions for a prismatic simply supported elastic beam were run so that natural periods of vibration determined using the time marching algorithm could be checked against closed form solutions. Addition comparisons were made with a symmetrically loaded generalized 1 degree of freedom beam model forced to vibrate as a half sine curve. The half sine curve represents free vibration in the fundamental mode of a uniform, simply supported beam and represents the total response occurring under two point symmetrical loading. The time dependent centerline deflection was obtained by using numerical integration of Duhamel's Integral to incorporate the effect of the applied forcing functions. Comparison of the responses calculated by the two analytical methods for the same symmetrical loading on the same beam showed good agreement when the higher mode vibrations occurring in the solutions using the finite difference time marching program were ignored.

Changing the size of the beam segments by using 11, 15, and 24 degrees of freedom for the time marching algorithm solutions had little effect, provided the time advance increment was made sufficiently small with increasing degrees of freedom. Too large a time increment made the algorithm unstable.

3.2 Parametric Study

A parametric study was undertaken to define relationships between forces, reactions, moments and deflections under dynamic loading. Since the variation of applied forces and beam properties may be quite large, a trial and error procedure was used to vary the parameters. The parametric study was also used to explain specific response patterns which

were recorded experimentally. The insight gained by studying the predicted response was invaluable in evaluating the observed response.

3.3 Basic Beam Model

The model beam used in the majority of the analytical studies is shown in Fig. 3.3. It was divided into 16 equal segments and had 15 degrees of freedom. Three segment lengths on each end were assumed uncracked with a moment of inertia of 4800 $in.^4$ The interior ten segments were assumed to have flexural cracks and a moment of inertia of 1400 $in.^4$ The number of segments used was established on the basis of solutions for beams with varying number of segments to optimize accuracy and computation time. The force F (t) was applied using adjacent node points, as shown in Fig. 3.3. The modulus of elasticity of the steel was taken as 29.2×10^6 psi and that of the concrete as 3.6×10^6 psi.

3.4 Forcing Function

Because the applied forces were not measured, the influence of changes in the analytical forcing functions was studied extensively. Force-time records from past studies [2,5] established guidelines for the characteristics of the forcing functions. The records were obtained from tests in which a falling mass impacted on a stationary cushioning device. Typical force-time curves are shown in Fig. 3.4. The cushioning device was a vermiculite concrete filled steel cylinder similar to the devices incorporated in the current tests. Differences between the forcing functions of the past studies and the beam tests were expected, since different size masses and drop heights were used. The effect of the displacement due to beam deflection, and the use of different piston diameters also influence the force-time relationship.

The basic forcing function considered in the analytical study is shown in Fig. 3.5. The force increases linearly with time to reach its maximum level of FMAX over a rise time of TR. The force remains constant at FMAX over the time TC and then decreases linearly to zero in a declining time of TD. To allow time lags between forcing functions applied at

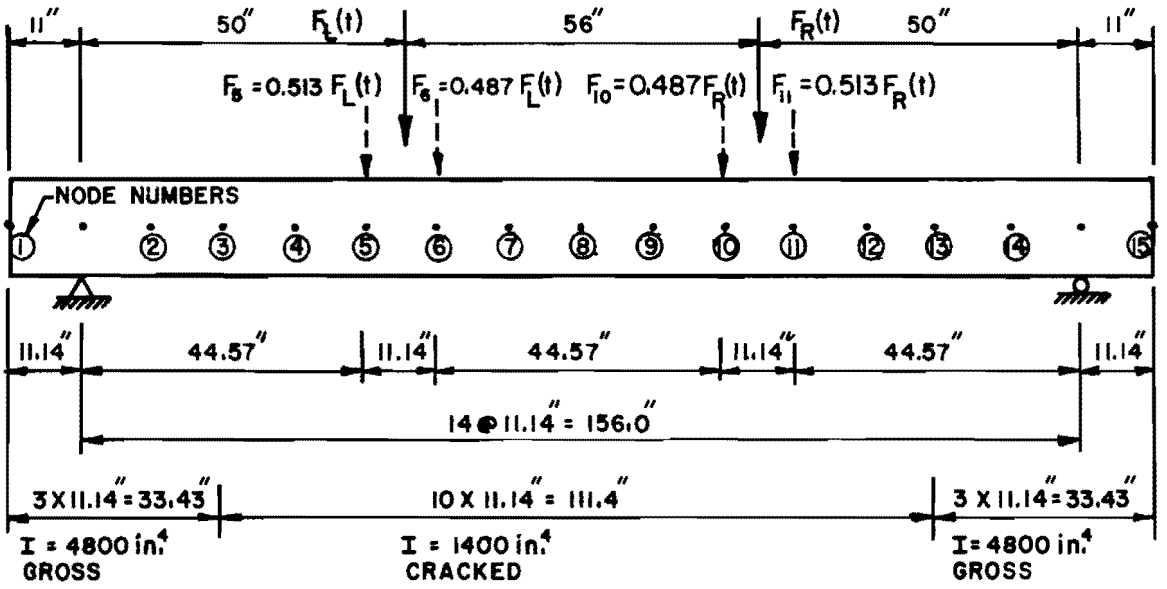

Nominal dimensions of test beams are shown above the beam (30 in. Splices). Node locations for model beam and assumed stiffnesses are shown below the beam.

LUMPED MASSES

$$\text{Segment weight} = \frac{(11.14\text{ in.})(15\text{ in.})(17\text{ in.})}{1728\text{ in.}^3/\text{ft.}^3} \times 150\text{ pcf} = 247\text{ lbs.}$$

$$\text{Segment mass} = \frac{0.319\text{ lb.-sec.}^2/\text{in.}}{247\text{ lb.}/32.2\text{ ft./sec.}^2}$$

Fig. 3.3. Dimensions and properties of the basic beam model

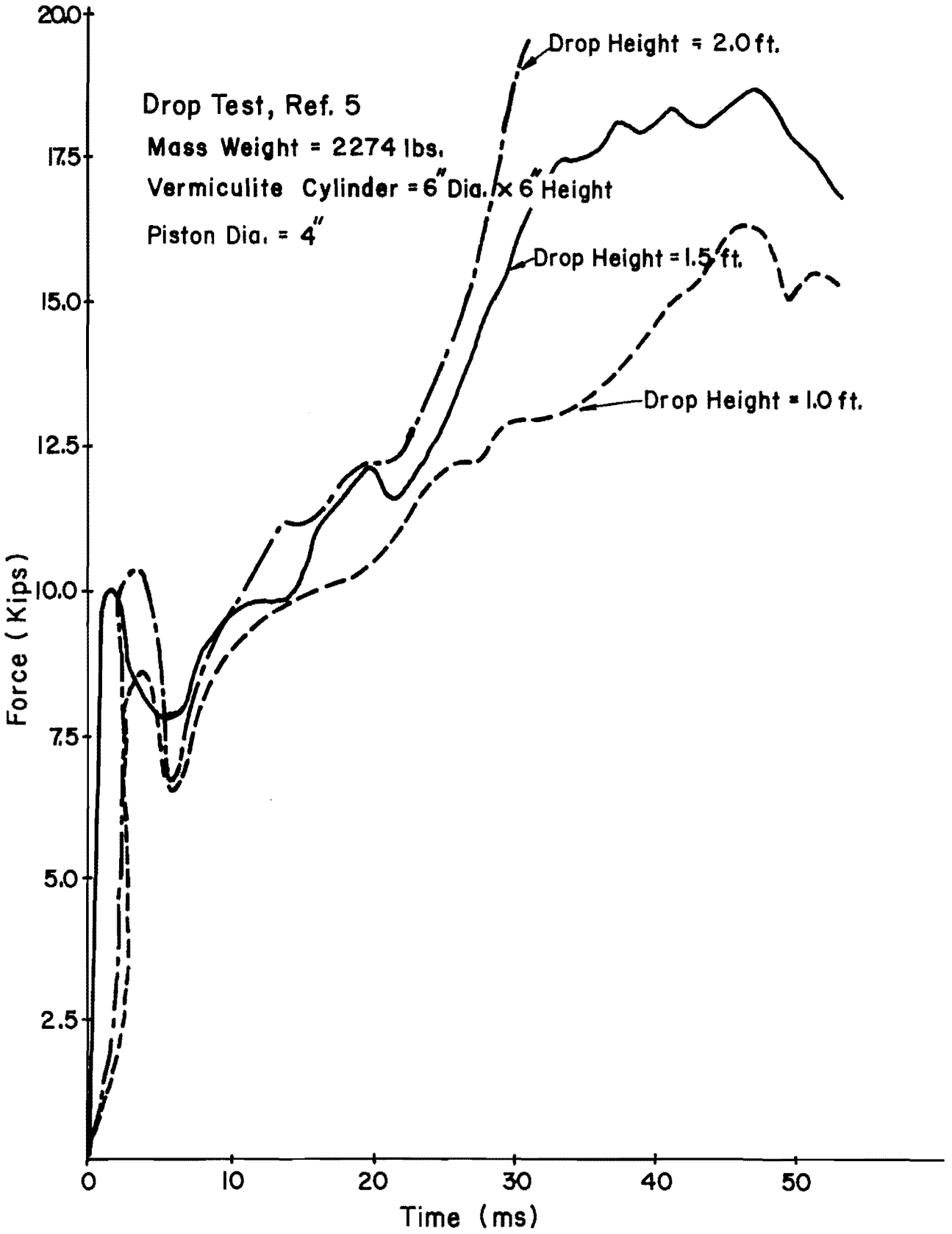

Fig. 3.4. Force-time curves - Ref. (5)

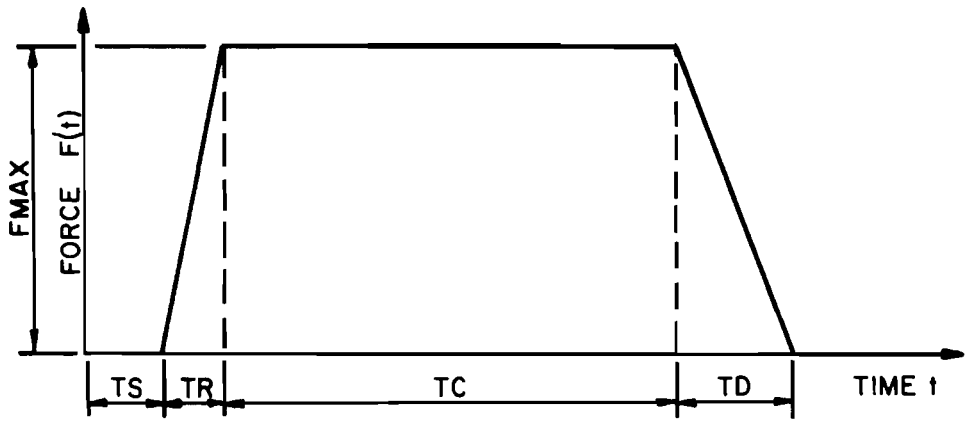

Fig. 3.5. Basic theoretical forcing function

different beam nodes a starting time TS can be used to offset the beginning of any forcing function from the overall reference time origin. The variables FMAX, TR, TC, and TS can be adjusted to study their effect on the analytical dynamic response.

The parameters describing the basic shape of the analytical forcing function in Fig. 3.5 were varied over wide ranges. Initially, identical forcing functions were used at the two load points to simulate simultaneous impact which resulted in symmetrical loading. The influence of varying rise time TR is shown in Figs. 3.6 to 3.8. The reaction, centerline moment, and centerline deflection are plotted. All parameters except TR remain constant: FMAX = 12000 lb., TC = 50 ms (0.05 seconds), TD = 5 ms, and TS = 0 ms (simultaneous impact on both points). The value of TR is 0.5 ms, 2.0 ms, 10.0 ms for the three cases. Rise times between 2 and 10 ms were considered typical for the test beams. Forcing functions are illustrated with dashed lines and have the same scale as the reactions. The basic beam shown in Fig. 3.3 was used to obtain the curves.

Examination of Figs. 3.6-3.8 reveals that the reactions for a rise time TR = 0.5 ms (Fig. 3.6) exhibit a higher mode vibration response

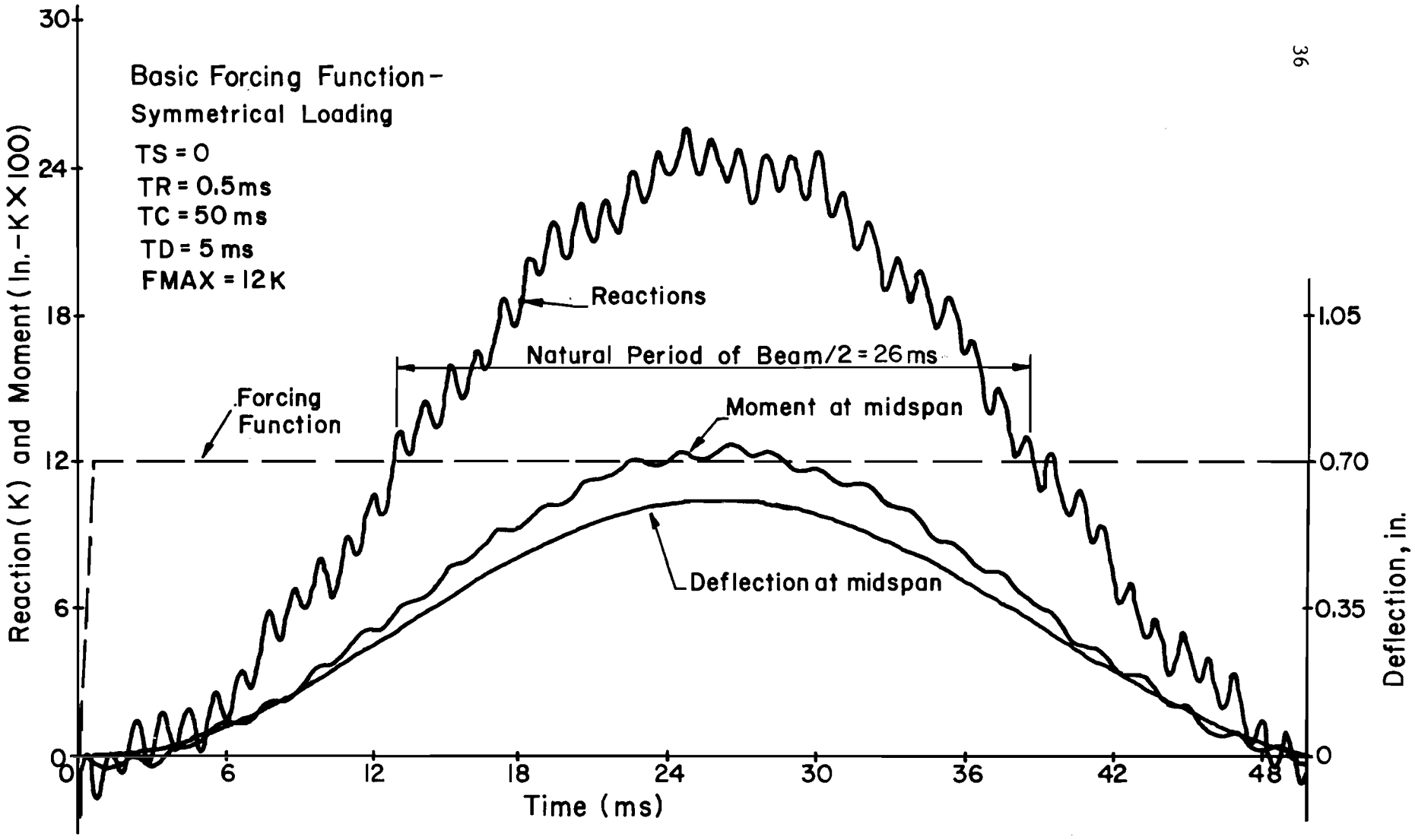

Fig. 3.6. Computed response - rise time = 0.5 ms

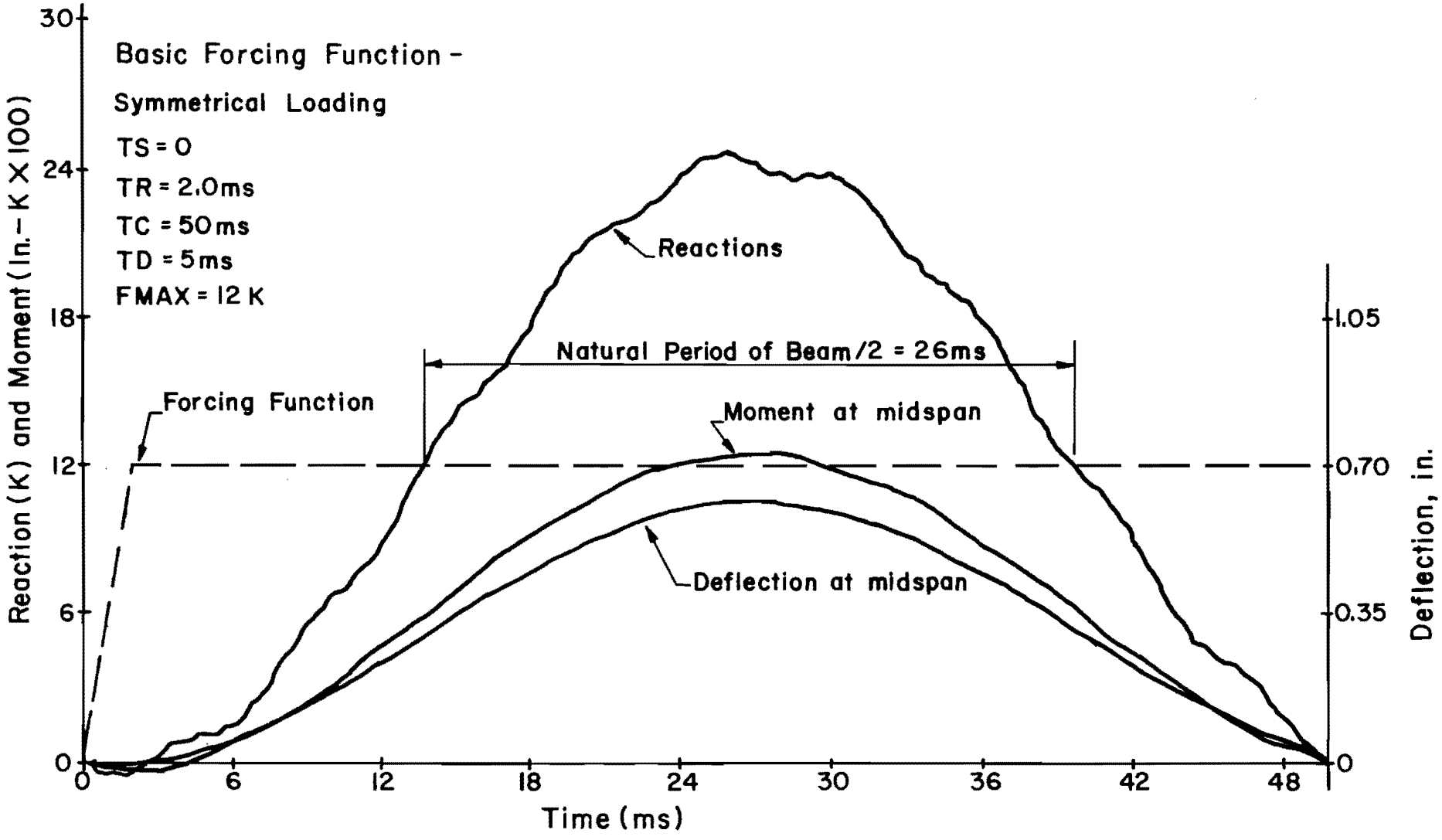

Fig. 3.7. Computed response - rise time = 2.0 ms

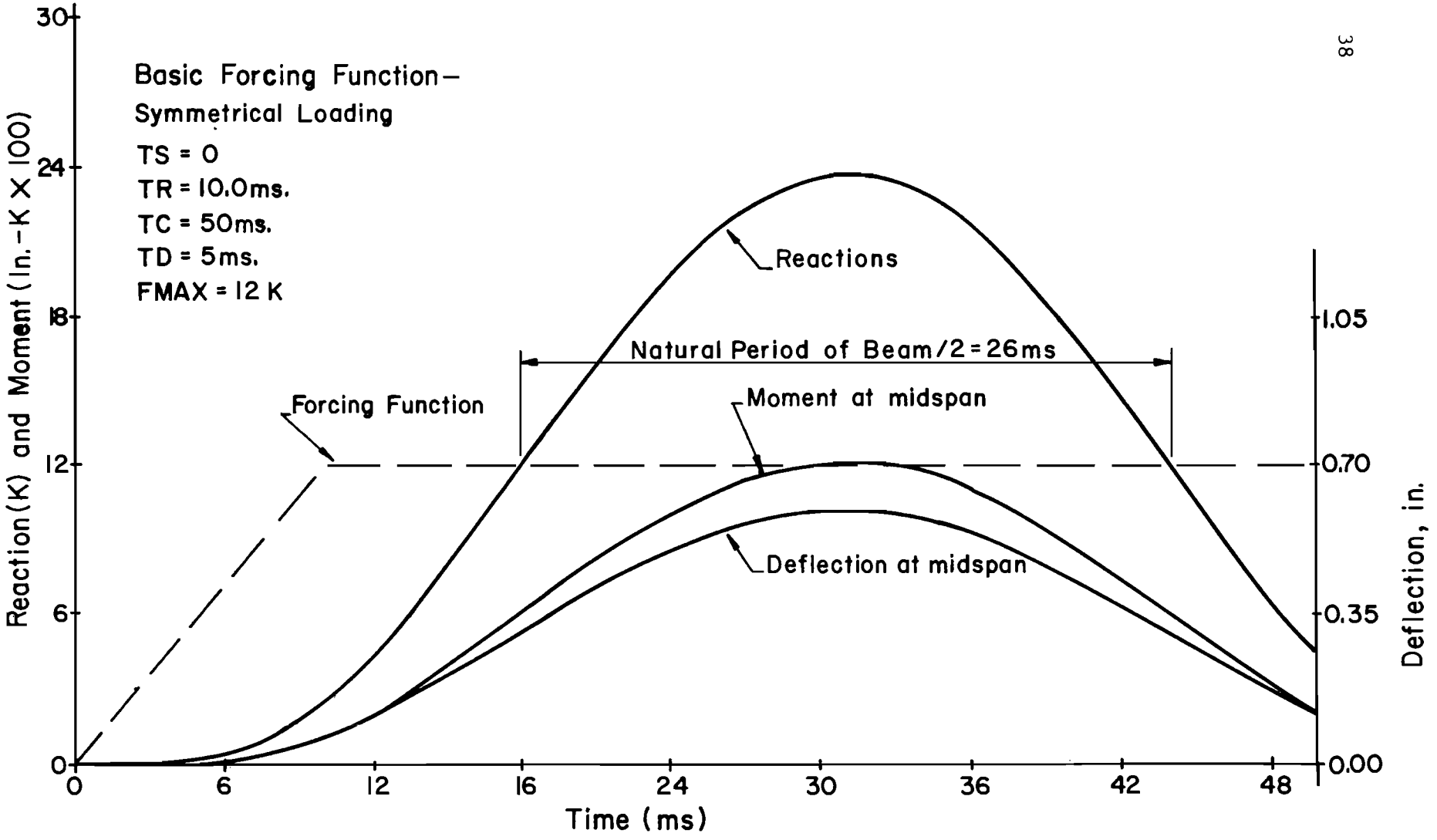

Fig. 3.8. Computed response - rise time = 10.0 ms

with a period of approximately 1.05 ms. With a rise time TR = 2.0 ms (Fig. 3.7), the higher mode response has a period of approximately 5.0 to 5.3 ms. With the rise times of 10 ms (Fig. 3.8) or longer, all higher modes of vibration in the reactions were suppressed and only the smooth fundamental mode is evident.

The higher mode response in the reaction shown in Fig. 3.6 is insignificant because a rise time of 0.5 ms is not likely to occur experimentally. The measured response from the test beams does not exhibit such a small period oscillation. Note that if the higher mode oscillations are ignored, the reaction and moment curves are nearly identical in all three cases, except that the peak magnitude is reached at a later time as the rise time increases. The deflection curves show no higher mode response in any case.

Over the time interval TC the reactions oscillate in the first natural mode about the base line established at the magnitude of the forcing function. The fundamental period for the model beam is approximately 52 ms and is noted in Figs. 3.6-3.8.

Force-time curves for the cushioning material (Fig. 3.4) indicate a rise time in the order of 2 to 5 ms, which is very small compared to the fundamental period of 52 ms. Large dynamic amplifications of the beam responses when compared to static loading were therefore expected in the experimental data. As a basis for investigating the effect of the rise time TR, the ratio of the maximum reaction (neglecting higher mode responses) to the maximum applied force FMAX = 12K was calculated. These ratios were 2.03, 2.03, 1.97, and 1.79 for rise times of 0.5, 2.0, 10.0, and 20.0 ms, respectively. For rise times up to 10.0 ms, the rise time has little effect on the beam response. Only the time at which maximum amplitudes are reached shifts further from the origin as rise times increase. The above ratios remained nearly the same if the rise times were kept constant, but the maximum force level FMAX was increased to 15K.

It is interesting to note that if the peak reaction is multiplied by the shear span (50 in.) the resulting moment is equal to the peak

moment at the midspan. For example, using the data from Fig. 3.7, R is about 24.3k, and the midspan moment is about 1250 in.-k. It can be assumed that the moment produced by the distributed dead weight of the beam is negligible. In addition, the ratios of moments at nodes 7 and 9 (Fig. 3.3) which lie 11.14 in. to either side of the beam centerline (node 8) to the moment at the centerline are 0.985 and 0.990. These values indicate that the moment remains relatively constant along the middle portion of the beam which is where the splice is located. Maximum deflections at either the beam centerline or the load points can also be determined by using the computed reaction magnitudes at both the reaction and load points to determine the moment diagram and then calculating deflections. This can be illustrated using the maximum reaction of 24.3k for the solution shown in Fig. 3.7 to calculate a centerline deflection of 0.619 in. The exact maximum deflection from the dynamic analysis is 0.609 in.

Though not included herein, studies were made where the values of the constant time TC and the decline time TD shown in Fig. 3.5 varied. The results showed these parameters did not substantially influence dynamic response; therefore, TC and TD were both eliminated as variables by using values of TC greater than the time interval over which analytical responses were studied.

Modification of the Basic Forcing Function. The basic shape of the forcing function given by Fig. 3.5 does not have a gradually increasing force over the time range TC as would appear warranted from the behavior of vermiculite cushioning (Fig. 3.4). A study was made into the influence of increasing the magnitude of the forcing function with time along the interval TC to establish whether the shape of the forcing function is important.

The four forcing functions shown for trials 1 to 4 in Fig. 3.9 were applied to the model beam (Fig. 3.3). The forcing functions are a combination of the basic forcing function and a sine curve added to produce a more gradually increasing force to the peak. The period for the sine curves is large to produce an increasing force over the entire 50 ms

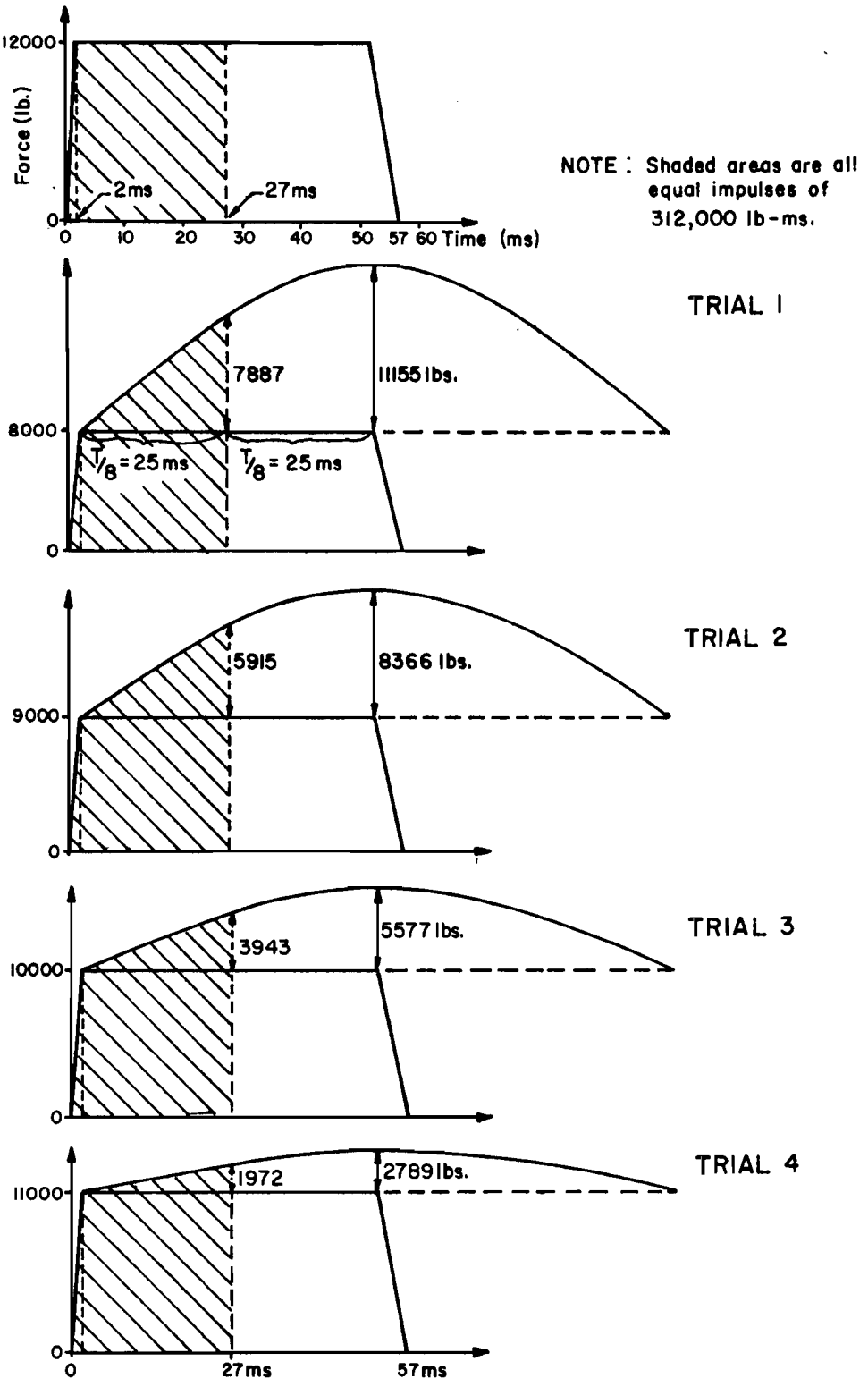

Fig. 3.9. Forcing functions with increasing magnitudes

time period studied. The forcing functions were proportioned so that the total area under the force time curves (impulse) up to a time of 27 ms would be equal to that for the basic forcing function with a 2 ms rise time. The impulse at 27 ms was chosen because it represents the time at which responses reach maximum values with constant FMAX = 12k and TR = 2 ms (Fig. 3.7).

The results showed that reactions, moments, and deflections at 27 ms (equal impulse) for all four trials were within 1 percent of values obtained with constant FMAX. To provide a measure of the amplification of reactions over the applied forces, the reaction divided by the applied force (FMAX) at the 27 ms time instant gave ratios between 1.53 for trial 1 to 1.87 for trial 4, compared with a value of 2.03 for constant FMAX.

Because forces were continually increasing to 27 ms, maximum responses were not reached at 27 ms, as were the responses for constant force. The amplification of the reactions under dynamic loading (reaction divided by force) was greatly influenced by the shape of the forcing functions. However, the relationship between reactions and moments closely approximated that for static loading. Therefore, it can be concluded that the inability to measure the applied load during testing was not a serious drawback. The impulse imparted by the forcing functions influenced reactions, but the shape of the forcing function was not important. Additional analytical studies did not consider continually increasing force magnitudes over the time interval TC.

Influence of a Time Lag (TS). The effects of nonsimultaneous impact of the two load points were studied because the test data often showed that the responses recorded did not always begin at the same time and higher modes often appeared to be related to the time lag. In particular, differences of up to 6 ms were occasionally observed in the times at which the two reactions began to increase. For a mass drop height of 18 in., a difference in the drop distance of 1/2 in. between the two ends of the beam results in a 4.25 ms difference in time of impact. Due to misalignment and possible drag along the guide rods of the drop mass, impact of one load point could easily occur while the mass was still 1/2 in. or more from impact at the second load point.

In the reaction traces shown in Fig. 2.5, higher mode vibrations with large amplitudes were observed. Study of the data for all test beams showed that the higher mode vibrations were not very regular, with amplitudes and periods varying not only between specimens and load cycles, but even within the same reaction of the same load application. For the beams with 30 in. splices, the period for the higher modes varied between 4 and 11 ms, with most in the 5 to 7 ms range.

A series of solutions using forcing functions with the general shape of Fig. 3.5 were made to explore the influence of time lags between the two load points. Beam properties were left unchanged from the ones used previously (basic beam). In addition to using different forcing function start times (TS) at the two load points, different magnitudes were assigned to the maximum force FMAX to model the probability that the two forcing functions would not reach equal levels, especially when impact was not simultaneous. Figures 3.10 to 3.12 illustrate the computed responses. The right forcing function had the following characteristics: TS = 0 ms, TR = 2 ms, and FMAX = 12k for all three cases. The left forcing function had TR = 2 ms and FMAX = 15k, but the start times TS were 0, 3, and 7 ms. Note that with no time lag (TS = 0), higher mode vibrations with a period of about 5 ms were present (Fig. 3.10). However, as the time lag between application of two forces increased to 3 ms or more, an unsymmetrical mode of vibration becomes very pronounced (Figs. 3.11 and 3.12). The period for the unsymmetrical mode is approximately 11 to 11-1/2 ms. It is interesting that on a few beam tests, reaction responses with higher mode vibrations around 11 ms were observed; however, most experimental data indicate a symmetrical mode with a smaller period.

Several features of the curves shown in Fig. 3.10 to 3.12 deserve comment. Moments and deflections did not exhibit a higher mode response corresponding to the unsymmetrical mode present in the reaction. The influence of different force magnitudes with the same rise time (TR = 2 ms) on the time at which reactions begin to increase rapidly is seen in Fig. 3.10. The left reaction begins to increase at about 3 ms, while the right reaction

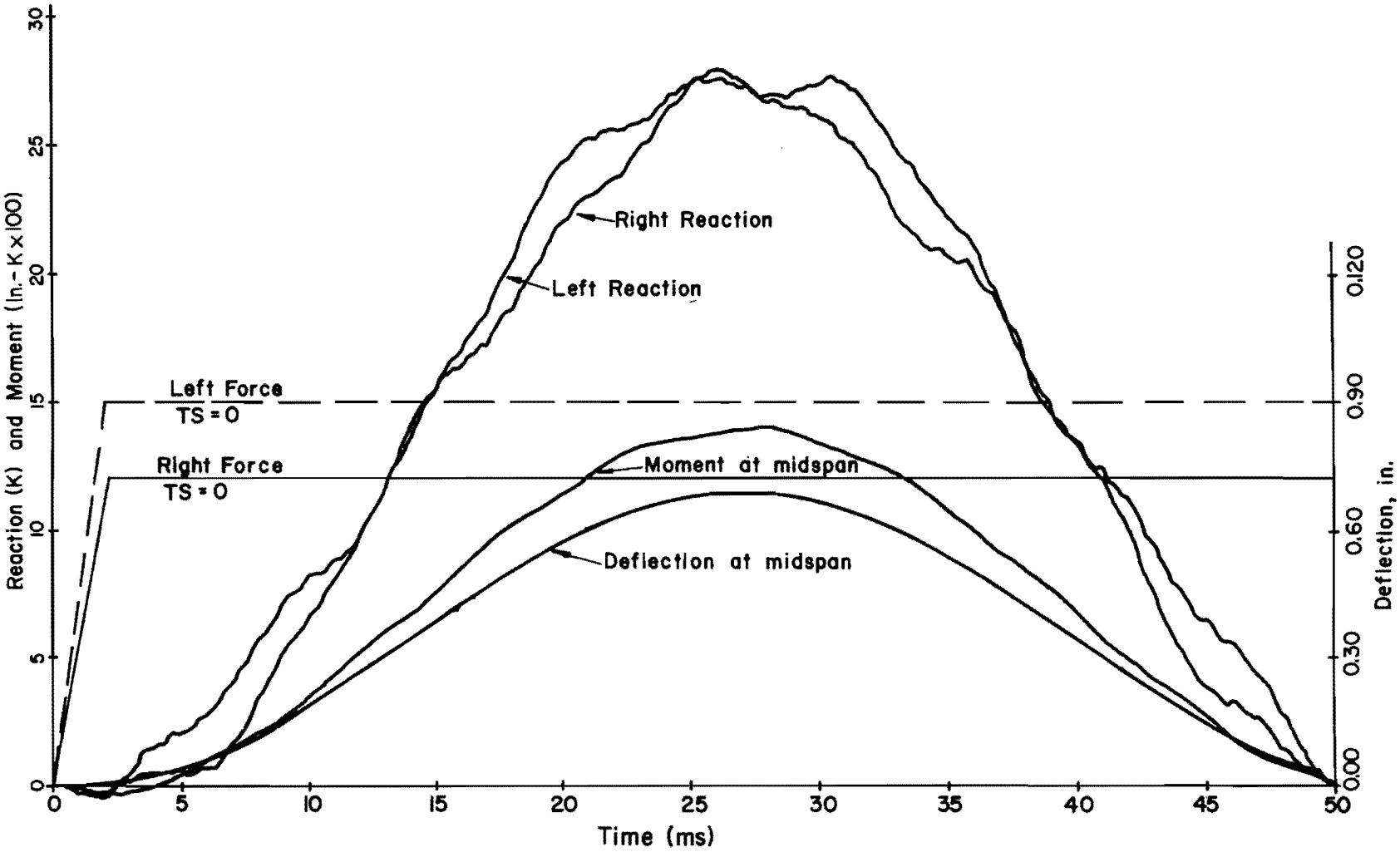

Fig. 3.10. Computed response - time lag = 0

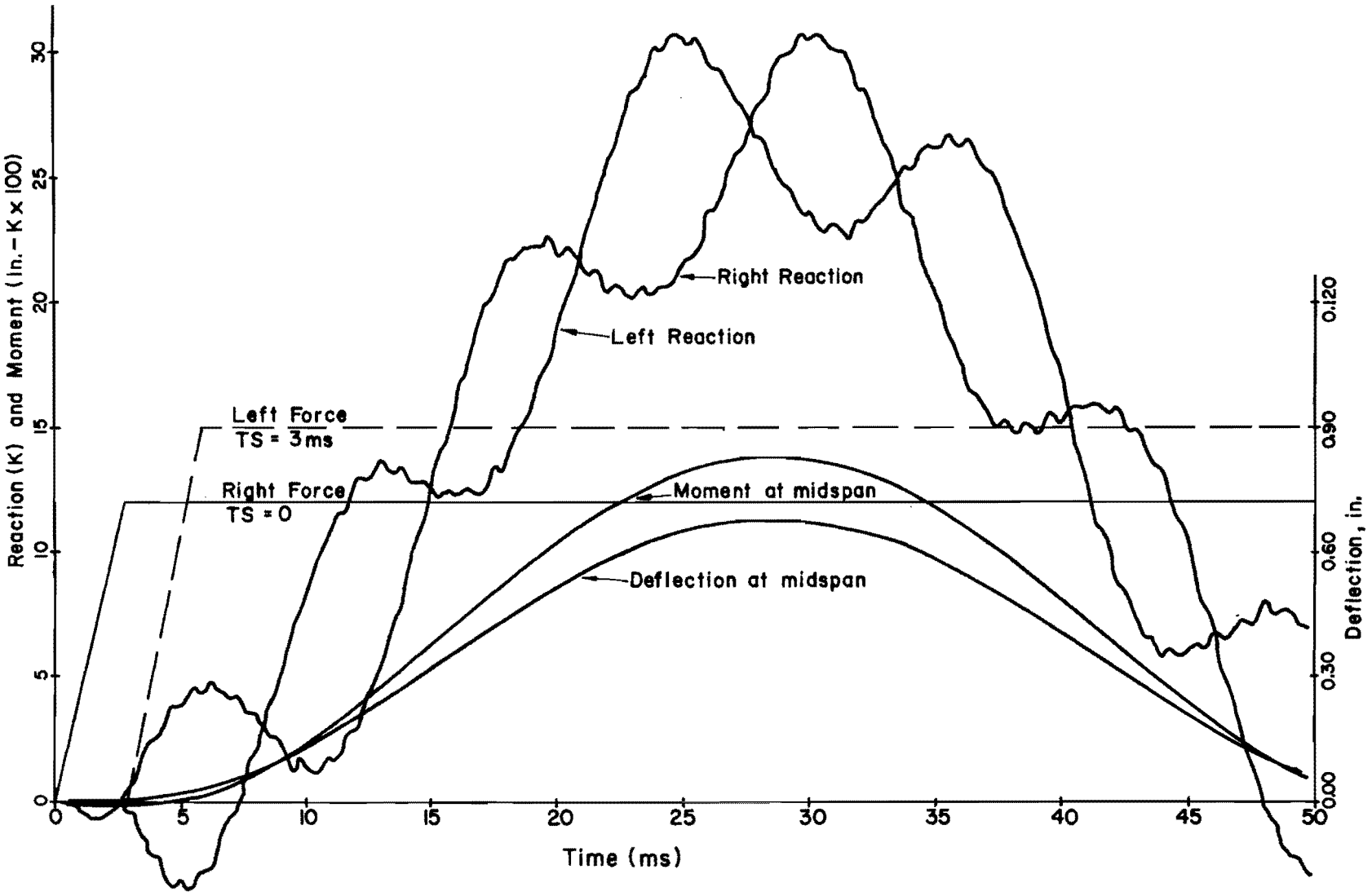

Fig. 3.11. Computed response - time lag = 3 ms

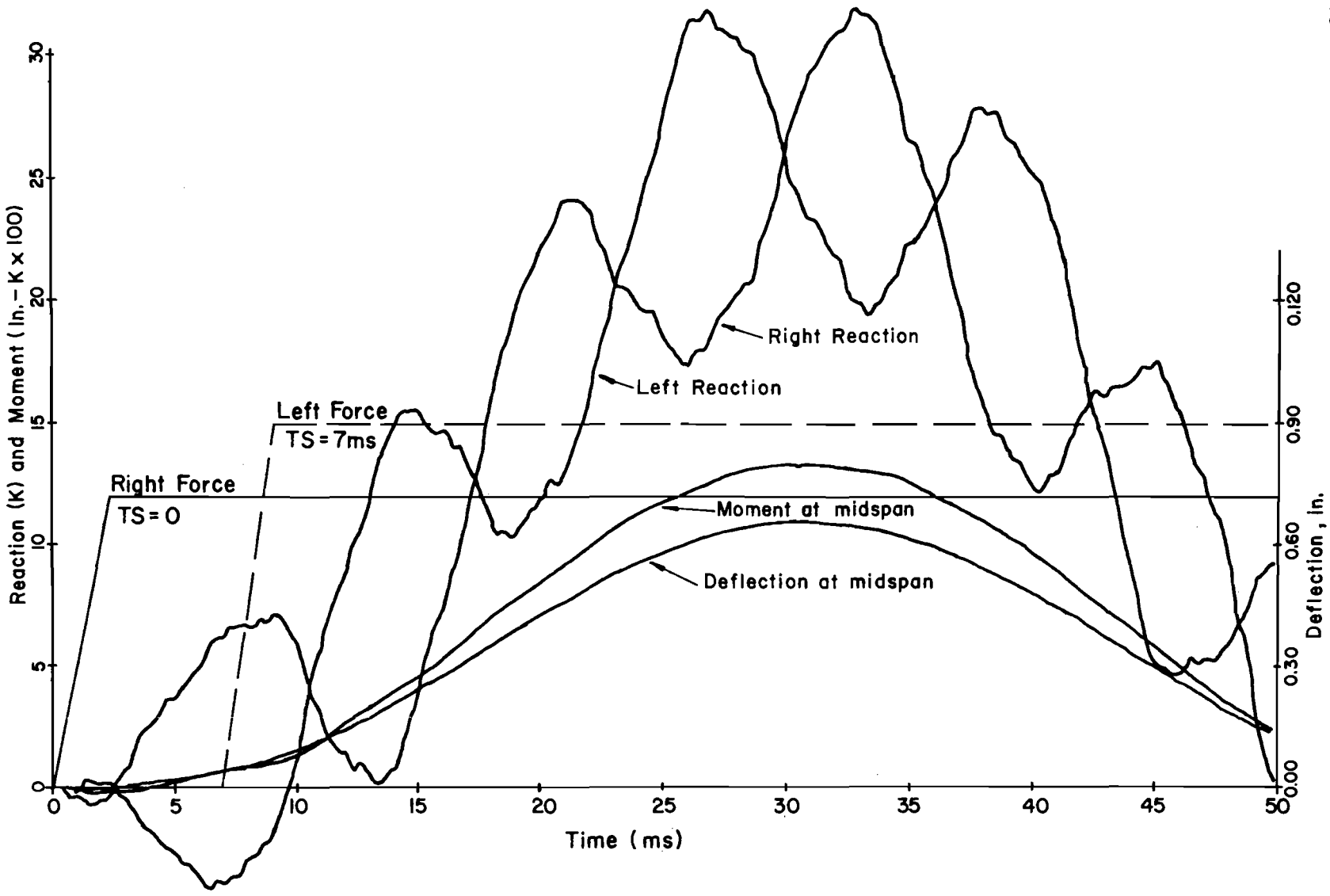

Fig. 3.12. Computed response - time lag = 7 ms

shows little change until about 6 ms after impact. This time lag of 3 ms in the reactions occurs without any time lag in the impacting forces, since both forcing functions start and reach their maximum values at the same times. If a time lag occurs in the forcing functions, larger time lags become apparent between the two reactions, as seen in Figs. 3.11 and 3.12. Negative left reactions occur shortly after impact (Figs. 3.11 and 3.12). Experimentally, the measured negative reaction could not exceed half the beam weight (2k) at which point the beam would lift off the reaction support. No attempt was made to model such behavior.

Initial Spike in the Forcing Function. Forcing functions with initial spikes, as shown in Fig. 3.13, were used in an attempt to amplify higher mode reaction responses with a period of about 5 ms. Figure 3.4 shows such spikes measured in studies of vermiculite cushioning. Peak amplitudes of up to 25 percent of the force level FMAX appear possible. A series of forcing functions were applied to the basic beam (Fig. 3.3). Starting times (TS), rise time (TR) and force levels (FMAX) were varied over the same ranges considered previously (TS = 0 to 10 ms, TR = 0.5 to 20 ms, and FMAX = 12k or 15k). The spike amplitude AMPSP was set at 0.25 times FMAX and its period TSP set at either 6 ms or 12 ms.

The computed response for a typical trial is shown in Fig. 3.13. The beam was loaded symmetrically with forces having TR = 2 ms, FMAX = 12k, AMPSP = 0.25 x 12 = 3k and TSP = 6 ms. The resulting reactions show little additional amplification of the desired higher mode vibration. Other trials showed the same results. It appears likely that spikes in the forcing functions were not the main cause of the large amplitude higher mode vibrations often found in the test data.

3.5 Influence of the Drop Mass

Several solutions were run to determine the influence of vibration of the drop mass on the higher mode vibrations observed in the experimental reaction data.

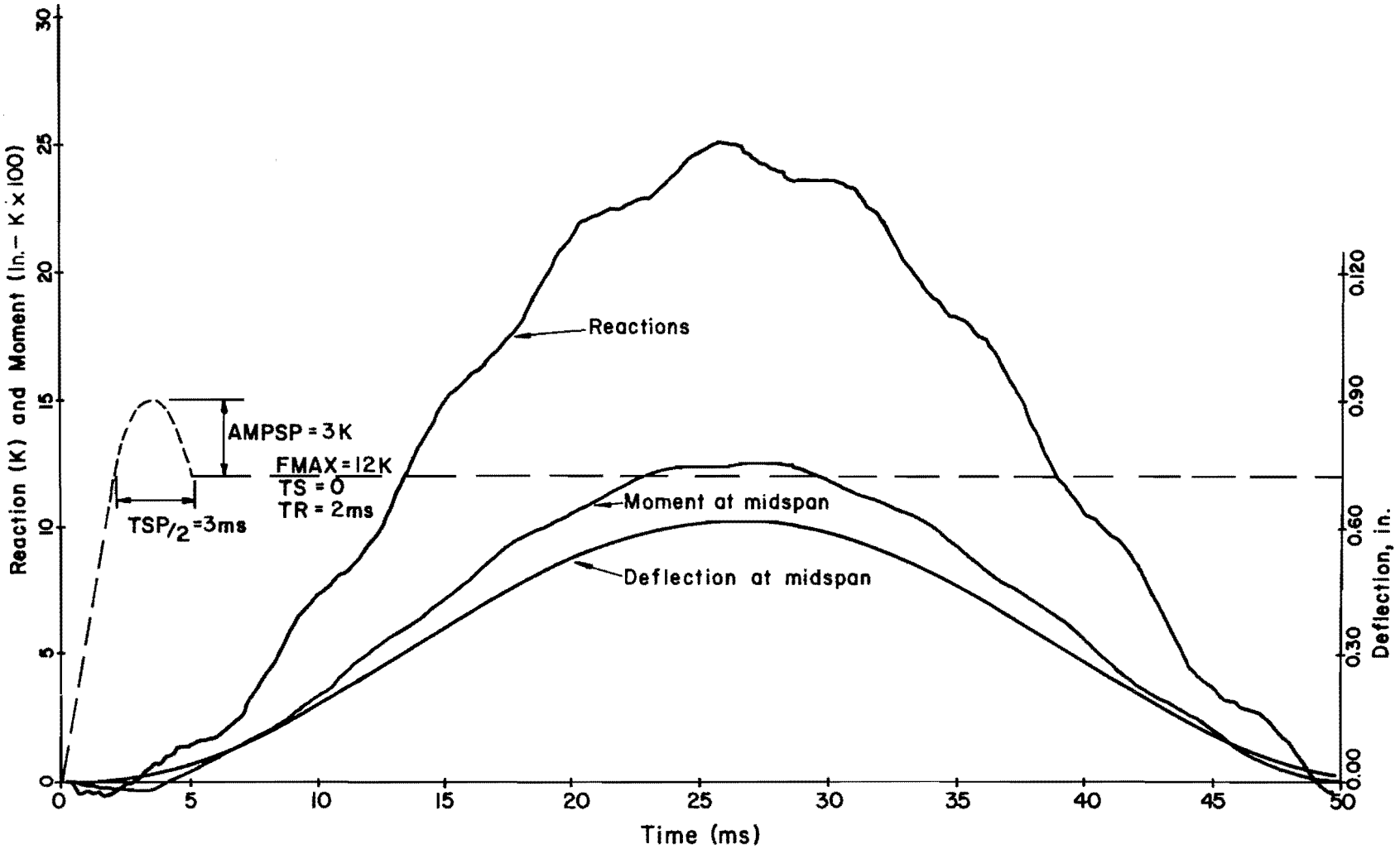

Fig. 3.13. Computed response - initial spike

The drop mass was treated as a uniform elastic beam with a moment of inertia of I = 8500 $in.^4$ and a uniformly distributed total weight of 2600 lbs. Pinned supports were assumed at the locations of the cushioning devices. The mass was discretized, as shown in Fig. 3.14 and loaded symmetrically with ramp forcing functions. Vibration modes with periods of 1.38 and 0.43 ms were excited by the symmetrical loading applied. Reaction responses consisted mainly of the higher mode variation while deflections followed the lower fundamental mode, as shown in Fig. 3.14.

It was assumed that the effect of vibration of the drop mass on beam responses could be included by modifying the forcing function to include a sinusoidal variation along the time interval TC, as shown in Fig. 3.15. Periods for this variation were taken as either 1.38 or 0.43 ms, the same as those of the drop mass. Symmetrical loadings with TR = 2 ms and FMAX = 12k were used. The amplitudes for the sinusoidal variation was set at 0.25 times FMAX. Reaction responses resulting from the loading with a 1.38 ms period excited a mode with a period of about 1 ms. The use of a 0.43 ms variation in the forcing functions gave an oscillation with a period of about 0.45 ms in the reactions. Therefore, it does not appear likely that the higher mode reaction vibrations recorded experimentally are caused by a vibration of the drop mass.

3.6 Variation in the Beam Stiffness

Numerous trials were run to investigate variations in the moment of inertia along the length of the beam while keeping the applied forces symmetrical with a constant maximum force level FMAX = 12k. For several trials using different rise times, the length over which the basic beam was assumed cracked was decreased by one segment length at each end. Other trials considered a moment of inertia of 2350 $in.^4$ over the central portion of the beam where the splice is located to account for the effect of the increased tension steel in that region. The basic beam properties were used for the remainder of the beam. Finally, several trials were made where the moment of inertia over the center region of the basic beam (Fig. 3.3) was reduced to 800 $in.^4$ to approximate a beam which had been extensively damaged and weakened by previous load applications.

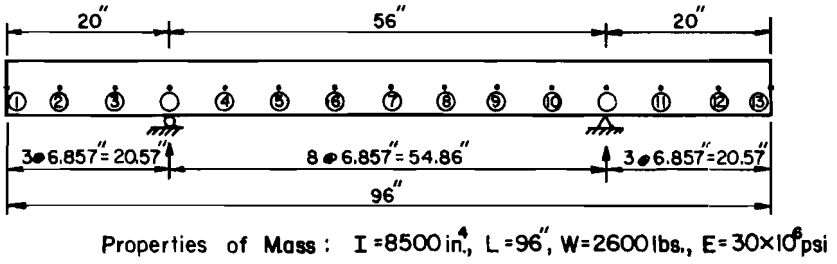

a) Model of the Drop Moss

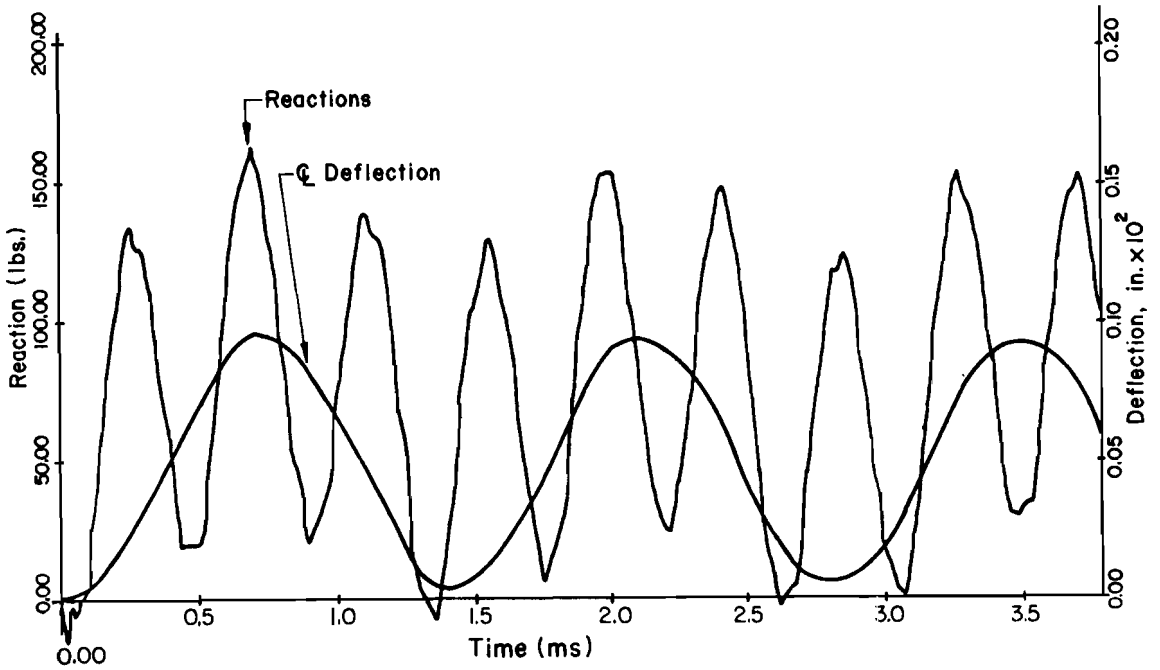

b) Dynamic Response of the Drop Mass

Fig. 3.14. Computed response - drop mass

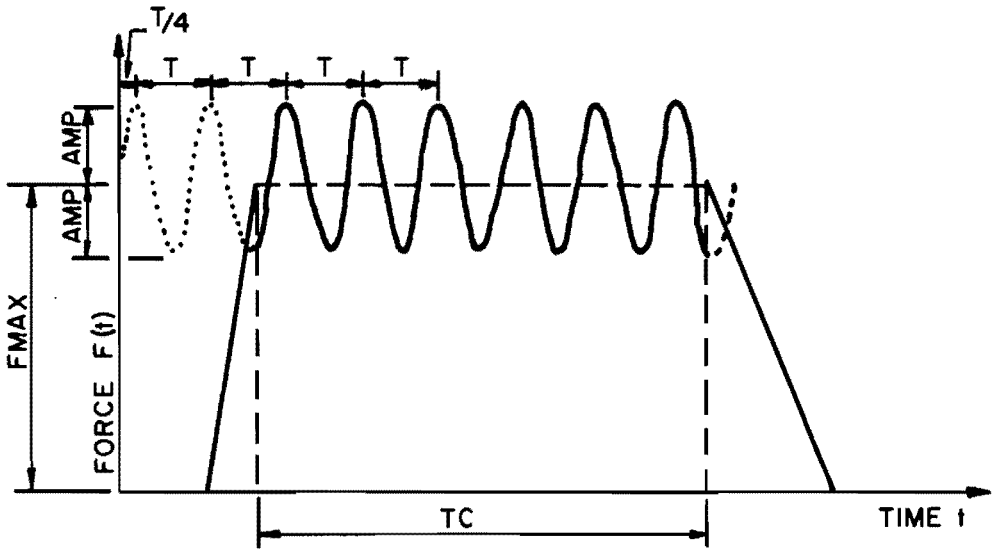

Fig. 3.15. Forcing function--modified for vibration of drop mass

For the same loadings, changing the beam stiffness produced the expected changes in the beam responses. The more flexible the beams, the larger the periods and deflections.

An illustration of the results of one of the trials is presented in Fig. 3.16. In this solution the moment of inertia of the basic beam (Fig. 3.3) was reduced from 1400 $in.^4$ to 800 $in.^4$ Note that the major change is in the fundamental period which increased from 52 ms to about 70 ms.

3.7 Influence of Inelastic Behavior

In an attempt to excite the vibration mode observed in the test data (5 ms period), a technique was developed to indirectly model degradation of stiffness produced by cracking, slip along the splice, or yielding. Inelastic behavior due to concrete cracking or other effects

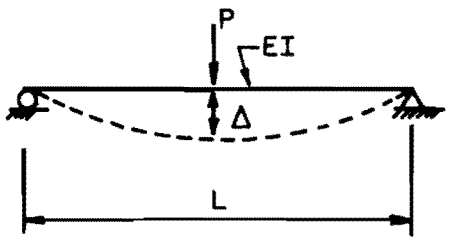

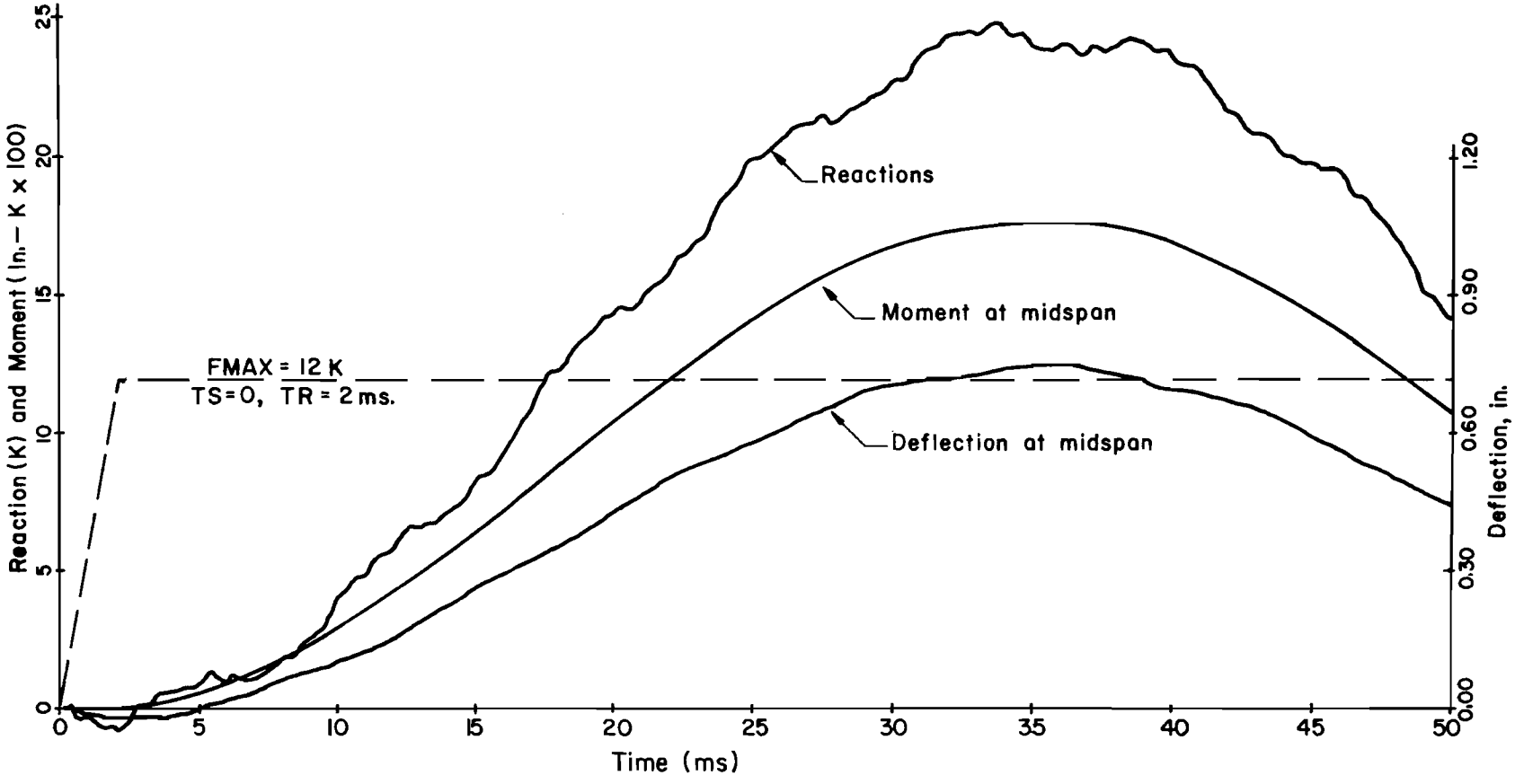

Fig. 3.16. Computed response - reduced beam stiffness

would reduce the effective beam stiffness, leading to an increase in deflection. This deflection can be simulated by rapidly and temporarily applying an external moment to portions of the beam where inelastic behavior is occurring. A series of trials were made where equal and opposite symmetrically placed moments were applied to the model beam. The computed reaction responses showed a higher mode vibration with a period of 5 to 7 ms. However, because of the difficulties in modelling inelastic behavior, it is difficult to assess the importance of this solution.

3.8 Summary of Analytical Results

The parametric study explored in detail variations in the load or forcing function, beam stiffness, and drop mass which could account for some of the responses observed in the test program. General response patterns from the experimental program were duplicated in the theoretical study. It was shown that the higher mode vibration effects could be eliminated in examining the test data. The maximum moment along the splice can be closely approximated by multiplying the maximum reaction by the shear span of the beam. The exact shape of the forcing functions does not appear to influence significantly the response of the beam.

CHAPTER 4

TEST RESULTS

4.1 Objectives

The overall objective of the study was to compare the dynamic behavior of a splice with static behavior. The maximum capacity of the splice under dynamic behavior was evaluated by determining the maximum bending moment carried at the spliced section.

The large volume of test data made condensation of the data mandatory. Therefore, only the maximum responses attained during an impact load are tabulated. Moments were obtained from reactions and steel strains and are included in the tabulations.

4.2 Typical Responses

Sample data traces were shown in Chapter 2. Characteristics manifested in the dynamic data were examined analytically and guidelines for analysis were established. Figure 4.1 further illustrates typical behavior during an impact load application. Responses are drawn on the same horizontal time axis so that a vertical line intersects all curves at the same time.

Recorded reactions display higher mode vibrations with a period of around 6 ms. Dashed lines show reaction curves which eliminate the higher modes.

The vertical line labeled "time instant for data analysis" identifies the time at which moments on the splice are at or near maximum values.

Strains 1 and 2 are measured at the splice ends and indicate yielding. The rapid drop in strain 2 after reaching a peak is indicative of unloading following yield. Strain 6 is measured at the center of the lap splice where yielding does not occur because the tensile steel area is doubled and moments are the same as at the end of the splice.

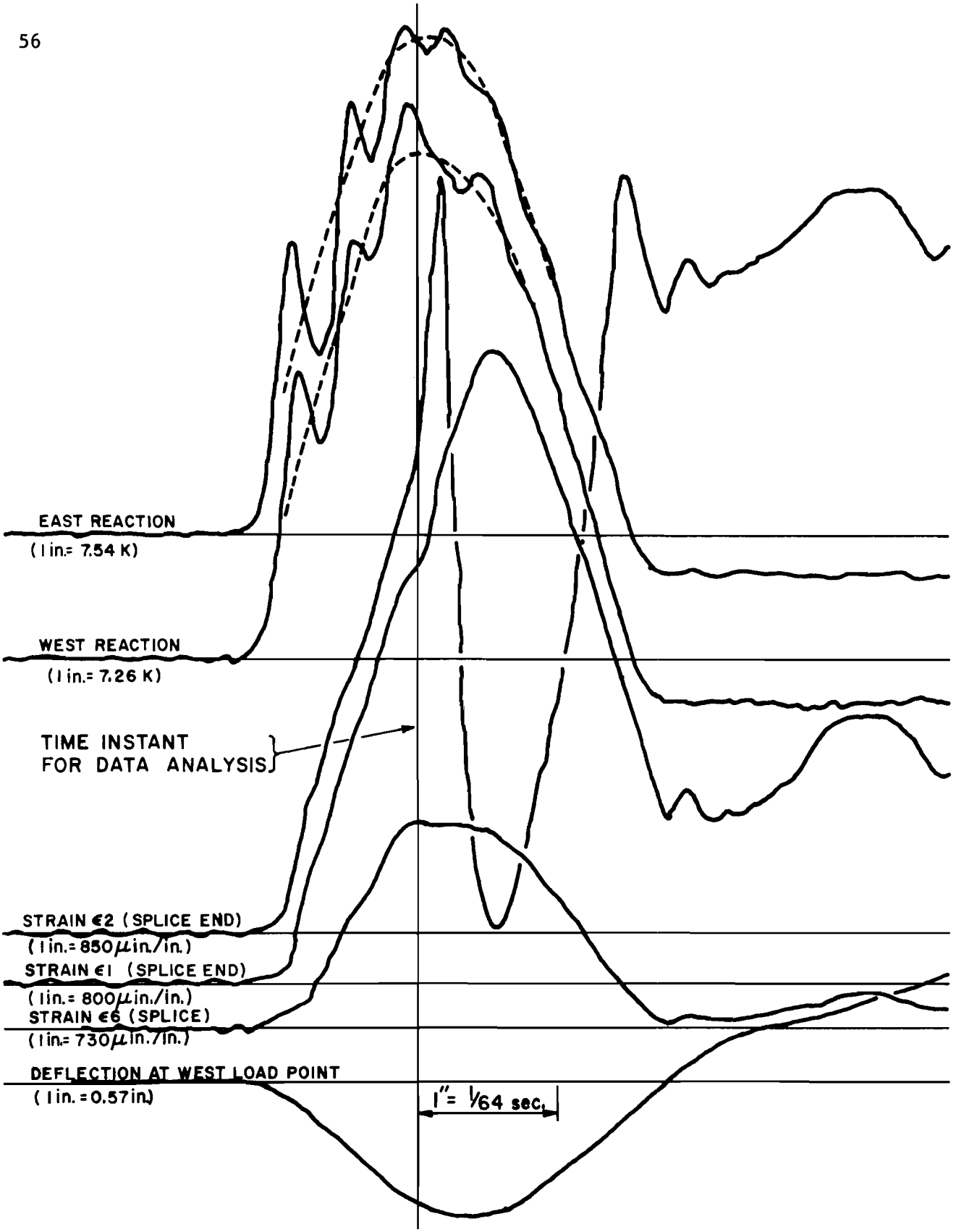

Fig. 4.1. Measured response for Specimen C-30-2T, load cycle 1, drop height = 18 in.

The smooth regular curve shown for the deflection at the west load point is typical. For the load cycle shown the maximum deflection occurs later than the time at which maximum reactions are reached.

For clarity Fig. 4.1 does not show all the data recorded in the test indicated. The following sections detail the methods used in determining values which appear in tabular summaries to reflect maximum dynamic capacity (strength) of the lap splices.

4.3 Data Tabulations

Data tabulated in Tables 4.1, 4.2, and 4.3 were determined from the response traces. For a given load cycle, responses are all tabulated at the same time (time instant for data analysis) and in general represent maximum magnitudes except for deflections and strains exceeding yield which often reach a maximum at a later time.

Table 4.2 includes both east and west reactions (RE and RW). The values are based on the traces resulting if higher mode vibrations are eliminated as shown by dashed lines in Fig. 4.1. The theoretical study discussed in Chapter 3 indicated that such approximations did not influence the moment acting on the beams.

Deflections at the two load points are averaged in the tabulations. Maximum deflections (ΔMAX) are also listed since deflection at the peak reaction was often not the maximum value recorded.

Strain readings were considered accurate until yielding occurred. Subsequent strains observed at a gage exhibiting yield are of questionable value. Strains tabulated are those at the time instant for data analysis. Average strains at the ends of the splice and at the midlength of the splice are listed with the number of gage readings included in the average noted. Provided all gages were in operation, four readings are averaged.

It should be noted that a number of checks were made on the reliability of the data. A detailed discussion of the data reduction procedure is contained in Ref. 12.

TABLE 4.1. TEST DATA - IO, IM SERIES

Specimen	Load Cycle	Drop Height in.	R_{avg} k	Δ in.	Δ_{max} in.	ϵ_E* μ in./in.	ϵ_c* μ in./in.	Moments, in.-k MR	Moments, in.-k Mϵ
IM-18	1	10	10.5					420	
	2	24	16.0	0.13	0.13	930	260_3	640	500
	3	28	33.8	0.36	0.38	2395_2	1145^3	1350	1300
	4	28	32.7	0.35		2410^2	1145^3	1310	1300
IO-18	1	45	32.6	0.41		2440	1140	1300	1300
IM-30	1	10	8.1	0.11	0.11			410	
	2	24	18.9	0.36	0.36	1685_3	730	950	910
	3	24	26.4	0.52	0.71	2540^3	1010	1320	1405
	4	40	28.2	0.58			1400^3	1410	
IO-30	1	45	27.2	0.59		2670	1020^3	1360	1440
IM-30T	1	8	8.5	0.07	0.07			430	
	2	24	17.5	0.28	0.28	1610	700^3	880	870
	3	24	26.2	0.50	0.60	2640	1060^3	1310	1420
	4	45	28.9	0.84	0.92		1130^3	1440	
	5	48	40.0	0.90	1.08		1180^2	1550	
	6	48	32.0	1.10	1.28			1600	
IO-30T	1	58	29.6	0.94	1.11	2530^3	1180^3	1480	1390
IM-42	1	9	8.4	0.18	0.18			500	
	2	24	17.5	0.49	0.49	1850	890^3	1050	1000
	3	32	23.6	0.64	1.01	2390	1090^3	1420	1290
	4	79	24.0	1.33	1.92		1140^3	1440	
IO-42	1	72	23.5	1.56	1.20	2620	940^3	1410	1370

*Strains ϵ_E at splice end, ϵ_c at midlength, superscripts refer to number of gages averaged if less than 4.

TABLE 4.2. TEST DATA - C SERIES

Specimen	Load Cycle	Drop Height in.	R_{avg} k	Δ in.	Δ_{max} in.	ϵ_E* μ in./in.	ϵ_c* μ in./in.	Moments, in.-k MR	Mϵ
C-18-1	1	24	24.6	0.37	0.38	1880	830	980	1010
	2	24	27.4	0.39	0.42	2070	950	1090	1110
	3	24	28.1	0.39		1940	980[3]	1120	1050
C-18-2	1	12	20.1	0.25	0.26	1290	460	800	700
	2	10	22.8	0.34	0.35	1670	730	910	900
	3	10	25.3	0.34	0.35	1800	800	1010	980
	4	8	22.7	0.31	0.32	1640	700	910	890
	5	8	24.5	0.34	0.36	1790	830	980	970
	7	8	26.1	0.38	0.39	1930	860	1040	1050
	9	8	25.6	0.42	0.43	1830	930	1020	990
	11	8	11.1					440	
C-18-3	1	16	21.9	0.31	0.35	1390	450[3]	880	750
	2	16	24.1	0.37	0.39	1670	760[3]	960	910
	3	16	27.0	0.41	0.44	1860	950[2]	1080	1000
	4	16	25.0	0.42	0.85	1660	855[2]	1000	900
	5	12	12.4	0.11				500	
C-30-1	1	10	21.0	0.40	0.41	1880[3]	640[3]	1050	970
	2	60	31.3	0.72	1.24	2480[3]	1110[3]	1570	1280
	3	60	31.1				1350[3]	1560	
C-30-2	1	18	26.2	0.53	0.56	2240	1190[2]	1310	1210
	2	18	28.3	0.58	0.63		1290[2]	1420	
	3	18	28.0	0.61	0.66		1270[2]	1400	
	4	18	27.4	0.61	0.67		1310[2]	1370	
	5	18	27.4	0.63	0.69		1260[2]	1370	
	6	18	25.1	0.63			1330[2]	1260	
C30-1T	1	14	24.0	0.47	0.50	2160	1000[2]	1200	1170
	2	72	30.1	1.17	1.52	2600	1300[2]	1510	1410
	3	72	35.8	1.09	1.12			1790	
	4	72	32.0					1600	
	5	84	25.0					1250	
C-30-2T	1	18	26.3	0.49	0.55	2430	1100[2]	1310	1370
	2	18	26.5	0.55	0.63	2610[3]	1190[2]	1320	1400
	3	18	27.0	0.62	0.68		1260[2]	1350	
	5	18	27.4	0.67	0.74		1320[2]	1370	
	10	18	28.3	0.74	0.79		1370[2]	1410	
	15	18	27.3	0.75	0.77		1440[2]	1360	
	18	18	25.7	0.79	0.84		1290[2]	1280	
	19	18	24.0	0.79	0.81		1180[1]	1200	
	20	18	18.7					935	

*Strains ϵ_E at splice end, ϵ_c at midlength, superscripts refer to number of gages averaged if less than 4.

TABLE 4.3. TEST DATA - CR SERIES

Specimen	Load Cycle	Drop Height in.	R_{avg} k	Δ in.	Δ_{max} in.	ϵ_E^* μ in./in.	ϵ_c^* μ in./in.	$\epsilon_{\epsilon R}^*$ μ in./in.	Moments, in.-k MR	Mϵ	MϵR
CR1-30	1	8	17.6	0.33	0.34			1590^2	880		820
	2	8	19.0	0.34	0.38	1650^3	730^2		950	850	
	5	8	21.6	0.42	0.43			1850^2	1080		1000
	6	8	22.0	0.42	0.43	1950^3	990^2		1100	1010	
	13	8	22.3	0.44	0.45				1110		
	14	8	23.5	0.42	0.43				1120		
	15	9	22.9	0.47	0.47			1940^1	1140		1050
	16	9	23.3	0.45	0.45	2090^3	1040^2		1110	970	
	17	9	22.8	0.48	0.48			2000^1	1140		1080
	18	9	23.3	0.45	0.45	1940^2	1080^2		1170	1050	
	19	10	24.5	0.50	0.50			2180^2	1220		1090
	20	10	23.6	0.49	0.49	2010^2	1100^2		1180	1090	
	23	10	24.3	0.55	0.55			2080^1	1220		1120
	24	10	23.0	0.51	0.52		1160^2		1150		
	25	24	26.2	0.71	0.83			2380^1	1310		1670
	26	24	26.3	0.81	0.90		1400^2		1320		
	27	84	32.0	0.89			1540^2		1600		
CR2-30	1	18	26.1	0.56	0.58	2330			1300	1260	
	2	18	26.3	0.65	0.69			2170^3	1320		1150
	3	18	25.2	0.66	0.72	2450^2			1260	1320	
	4	18	25.4	0.69	0.75			2420^3	1270		1240
	5	18	24.2	0.74	0.78				1210		
	6	18	25.0	0.77	0.83				1250		
	7	18	24.1						1210		
	8	18	15.9						800		
CR1-30T	1	18	25.0	0.56	0.58	2300	1110^2		1250	1240	
	2	18	27.0	0.65	0.68				1350		
	17	18	23.9	0.84	0.89		1360^2		1190		
	18	18	24.7	0.86	0.90				1240		
	19	21	25.2	0.89	0.92		1400^2		1310		
	20	21	24.6	0.95	0.98				1330		
	25	21	25.2	0.95	0.96		1380^2		1260		
	26	21	24.5	0.97	1.00				1220		
	27	24	25.3						1270		
	28	24	25.8						1290		
	31	24	25.9	1.03	1.07				1290		
	32	24	24.9	1.09	1.12				1250		
CR2-30T	1	18	25.0	0.58	0.60	2390			1250	1340	
	2	18	25.1	0.67	0.76			2670^2	1260		1440
	3	18	24.4	0.68	0.72				1220		
	4	18	24.5	0.71	0.78				1230		
	7	18	24.8	0.75	0.80				1240		
	8	18	24.5	0.86	0.87				1230		
	9	21	25.7	0.82	0.90				1280		
	10	21	24.1	0.92	0.95				1210		
	11	24	26.2	0.94	0.98				1310		
	12	24	24.3	1.04	1.09				1220		
	13	24	20.7						1040		

*Strains ϵ_E at splice end and ϵ_c at midlength at bottom splice, $\epsilon_{\epsilon R}$ at splice end of top bar. Superscripts refer to number of gages averaged if less than 4.

Moments along the splice were calculated from reactions and strains. The average of the two reactions was multiplied by the shear span to give the moment (MR). The theoretical study in Chapter 3 showed that the dynamic moment along the splice could be calculated using the reaction, with higher mode vibrations neglected, multiplied by the shear span. Moments were calculated from steel strains using straight-line theory. Strains were converted to stresses using a modulus of 29.2×10^6 psi. The internal moment arm was taken as jd = 0.9d = 11.7 in. Moments are shown for the section through the end of the splice ($M\epsilon$). For the beams subjected to cyclic reversals (CR Series), the moment computed from strains measured on the top bars is noted as $M_{\epsilon R}$. If the top bars were spliced the moment is at the end of the splice. If the top bars were continuous, the moment is at a section coinciding with the end of splice on the bottom bars.

CHAPTER 5

EVALUATION OF CAPACITY OF A LAP SPLICE UNDER IMPACT LOADS

5.1 INTRODUCTION

A lap splice failure is generally characterized by splitting of the concrete cover surrounding a splice with an accompanying loss of stress transfer capacity. Modes of failure of splices are discussed in detail in Ref. [12]. Design philosophies require that failure be prevented, if possible, in order to allow a more favorable ductile behavior to develop. Ductile behavior provides a warning of structural distress through large deformations which absorb energy and redistribute forces from sections with high stresses to those at lower stress. Current recommendations and codes (based on static loading studies) require a splice length sufficient to develop stresses considerably in excess of yield. For a splice in a high stress region, Ferguson and Krishnaswamy [6] recommend a splice length of 1.3 times that needed to yield the bar to ensure a ductile flexural failure.

As previously shown, current ACI [1] and AASHTO [11] specifications require 47.1 in. and Ferguson and Krishnaswmy [6] recommend 51.5 in. for splices in #8 bars with geometry as in the current study with Grade 60 steel, f'_c = 3000 psi, and Class C designation (all bars spliced, $f_s > f_y$). Longer lengths are needed if the bar classifies as top reinforcement. Long splice lengths are essential in design but cannot be used in tests for studying splice behavior. Even the 30 in. splice length used in the majority of the test specimens was too long to allow a splice failure to occur in several of the specimens which had stirrups in the splice region.

To compare static and dynamic behavior of lap splices, it is necessary to compare maximum strengths reached under both loading methods. Since higher capacities were always found under impact loading, strain rates were examined to determine effects on material characteristics.

5.2 Splice Strengths - Static Loading

The moment capacities found in the reference static tests (RS Series) and the statically tested specimen of the current study (C-18-S) are tabulated in Table 5.1. The maximum splice moments were adjusted to reflect the influence of concrete strength on the splice failure mechanism where the tensile splitting produces failure. Since tensile strength is a function of the square root of the ultimate concrete compressive strength ($f_t \alpha \sqrt{f'_c}$), adjusted moments (M_{max}^*) were obtained by multiplying the measured moments (M_{max}) by the ratio ($\sqrt{3000}/\sqrt{f'_c}$).

TABLE 5.1. SPLICE STRENGTH - STATIC LOADING

Specimen	f'_c ksi	f_y ksi	$f_{s\,max}$ Measured ksi	M_{max} in.-k	M_{max}^* in.-k		$\frac{M_{max}^*}{M_{max}^*(18\text{ in.})}$
RS-18	3470	75	42.4	784	728	776	1.00
C-18-S	3330	60	47.0	868	824		
RS-30	3030	75	52.5	970	965		1.24
RS-30T	2610	75	57.3	1060	1135		1.46
RS-42	2660	75	66.2	1224	1300		1.67

*Adjusted for nominal f'_c = 3000 psi.

Note: All specimens failed in the splice.

Increase in moment capacity with splice length is clear, with the 42 in. splice 67 percent stronger than the average of the strengths of the 18 in. splices. The increased capacity obtained by using stirrups is seen in the moment ratios of the 30 in. splices. Specimen RS-30 (no stirrups) is only 24 percent above the 18 in. splice capacity, while Specimen RS-30T (with stirrups) is 46 percent stronger.

5.3 Splice Strength - Impact Loading

Strengths of specimens subjected to impact loading are tabulated in Tables 4.1, 4.2 and 4.3. Moments calculated from reactions and from steel strains are listed. Table 5.2 compares moments carried along the splice for specimens under static and dynamic load.

The drop details list the drop height-piston diameter-vermiculite cylinder height, all in inches. The moment is obtained by multiplying the R_{avg} (from Tables 4.1 - 4.4) by the shear span and adding in dead weight moments of 40, 60, and 90 in.-k for specimens with 18, 30 and 42 in. splices respectively. Moments from strains were not considered in the comparisons.

The failure moment for the reference static tests adjusted for concrete strength is noted as M_s. The value of M_s is a function of concrete strength because all beams tested statically failed in the splice and the moment was not limited by yielding in the steel. For example the static moment capacity for specimen IM-18 is obtained as follows: $M_s = 776x(\sqrt{3180}/\sqrt{3000}) = 800$ in.-k. The moment of 776 in.-k is obtained from Table 5.1 and is the average static strength of two specimens with 18 in. splices.

The ratio M_D/M_s always exceeded 1.0 at some point in the testing sequence. Peak dynamic moments increased with increasing drop heights. For specimens with 18 in. splices, the maximum moment ratios are 1.33 for an 8 in. drop, 1.35 for a 16 in. drop, 1.41 for a 24 in. drop and 1.69 for a 48 in. drop. In all cases a 6 in. diameter piston and a 6 in. high vermiculite cylinder were used. The trend is similar though not as well defined for the specimens with 30 in. splices. For similar drop heights (30 in. splices) the moments are generally lower for reversed loading (CR Series) compared to unidirectional loading. This is likely due to the residual deflection from the previous load application. In each case, the residual upward deflection had to be overcome before net positive deflection occurred and as a result less energy from the impact was available for the remainder of the loading cycle.

TABLE 5.2. COMPARISON OF DYNAMIC AND STATIC SPLICE STRENGTH

Specimen	f'_c	Cycle No.	Drop Details	M_D in.-k	M_s in.-k	$\frac{M_D}{M_s}$	$\frac{M_D}{M_y}$
IM-18	3180	1	10-3-6	460	800	0.58	0.39
		2	24-4-8	680		0.85	0.58
		3	28-6-4	1390		1.74	1.19
		4	48-6-6	1350		1.69	1.15
IO-18	3180	1	45-6-6	1340	800	1.68	1.15
C-18-1	3330	1	24-6-6	1020	820	1.24	0.92
		2	24-6-6	1140		1.39	1.03
		3	24-6-6	1160		1.41	1.05
C-18-2	3400	1	12-6-6	840	830	1.01	0.76
		3	10-6-6	1050		1.27	0.75
		4	8-6-6	950		1.14	0.86
		7	8-6-6	1100		1.33	0.99
		11	8-6-6	480		0.58	0.43
C-18-3	3400	1	16-6-6	920	830	1.11	0.82
		2	16-6-6	1000		1.20	0.90
		3	16-6-6	1120		1.35	1.01
		5	12-6-6	540		0.65	0.49
IM-30	3160	1	10-3-6	470	990	0.47	0.90
		2	24-4-8	1010		1.02	0.86
		3	24-6-4	1380		1.39	1.18
		4	40-6-6	1470		1.48	1.26
IO-30	3160	1	45-6-6	1420	990	1.43	1.21
C-30-1	4060	1	10-6-6	1120	1130	0.99	1.01
		2	60-6-6	1630		1.44	1.46
		3	60-6-6	1620		1.43	1.46
C-30-2	4060	1	18-6-6	1380	1130	1.22	1.24
		2	18-6-6	1480		1.31	1.33
		6	18-6-6	1320		1.17	1.19
IM-30-T	3610	1	8-3-6	490	1245	0.39	0.42
		2	24-4-8	940		0.76	0.80
		3	24-6-4	1370		1.10	1.17
		4	45-6-6	1510		1.21	1.29
		5	48-6-5	1570		1.26	1.34
		6	48-6-7	1660**		1.33	1.42

TABLE 5.2 (Continued)

Specimen	f'_c	Cycle No.	Drop Details	M_D in.-k	M_s in.-k	$\frac{M_D}{M_s}$	$\frac{M_D}{M_y}$
IO-30T	3610	1	58-6-7	1540**	1245	1.24	1.32
C-30-1T	3820	1	14-6-6	1260	1280	0.98	1.14
		2	72-6-6	1570		1.23	1.41
		3	72-6-6	1850		1.45	1.66
		4	72-6-6	1660		1.30	1.50
		5	84-6-6	1310		1.02	1.18
C-30-2T	3820	1	18-6-6	1380	1280	1.08	1.24
		10	18-6-6	1480		1.16	1.33
		18	18-6-6	1350		1.05	1.22
		19	18-6-6	1260		0.98	1.14
		20	18-6-6	1000		0.78	0.90
IM-42	3260	1	9-3-6	590	1360	0.43	0.50
		2	24-4-7	1140		0.84	0.97
		3	32-6-5	1510		1.11	1.29
		4	79-6-6	1530**		1.13	1.31
IO-42	3260		72-6-6	1500**	1360	1.10	1.28
CR1-30	4320	1	8-6-6	940+	1160	0.81	0.76
		2	8-6-6	1010		0.87	0.91
		13	8-6-6	1170		1.01	1.05
		17	9-6-6	1200		1.03	1.08
		23	10-6-6	1280		1.10	1.15
		25	24-6-6	1370		1.18	1.23
		27	84-6-6	1660		1.43	1.50
CR2-30	4320	1	18-6-6	1370	1160	1.18	1.23
		2	18-6-6	1380		1.19	1.24
		6	18-6-6	1310		1.13	1.18
		8	18-6-6	860*		0.74	0.77
CR1-30T	3340	1	18-6-6	1310+	1200	1.09	1.18
		2	18-6-6	1410		1.18	1.27
		17	18-6-6	1260		1.05	1.13
		26	21-6-6	1290		1.08	1.16
		31	24-6-6	1360		1.13	1.23
		32	24-6-6	1310**		1.09	1.18

TABLE 5.2 (Continued)

Specimen	f'_c	Cycle No.	Drop Details	M_D in.-k	M_s in.-k	$\frac{M_D}{M_s}$	$\frac{M_D}{M_y}$
CR2-30T	3340	1	18-6-6	1310	1200	1.09	1.18
		8	18-6-6	1280		1.07	1.15
		9	21-6-6	1350		1.13	1.22
		10	21-6-6	1270		1.06	1.14
		11	24-6-6	1370		1.14	1.23
		12	24-6-6	1280		1.07	1.15
		13	24-6-6	1100*		0.92	0.99

Note: Drop Details - Drop Height, in.; Piston diameter, in., Vermiculite cylinder height, in.

**Splice did not fail.

*Top splice in tension.

+Top splice in tension on first load cycle.

Because the dynamic capacity exceeds static values by substantial amounts in most cases, M_D is compared with static yield strength. Ratios of M_D/M_y are listed in Table 5.2. The yield moment M_y = 1170 in.-k for IO and IM series beams (f_y = 63.3 ksi and jd = 0.9d), and M_y = 1110 in.-k for the C and CR series beams (f_y = 60 ksi and jd = 0.9d).

The ratios M_D/M_y illustrate the influence of yielding of the steel and should be studied in conjunction with ratios M_D/M_s in which the static moment is independent of the steel strength. For 18 in. splices, the dynamic moment achieved was as much as 19 percent over the static yield moment for the large drop heights. It should be noted that the number of load applications required to produce a splice failure decreased with increased drop heights.

For the 30 in. splices, the highest ratio of M_D/M_y was 1.66 for the third load cycle of Specimen 30-C-1T, however, most of the ratios were between 1.2 and 1.4. The failure drop height of 84 in. on CR1-30 was the largest in any test. It is interesting to note that the specimen was subjected to a large number of cycles prior to the 84 in. drop (24 total, with 12 producing tension on the splice) at loads near the static capacity, however, the splice strength does not appear to have been adversely influenced by the prior loading.

Specimens with stirrups along the splice fared better as expected. Of the six specimens with stirrups tested dynamically, Specimens C-30-1T, C-30-2T and CR2-30T failed in the splice. Specimen CR2-30T contained splices in the top reinforcement and will be discussed later. The remaining two specimens which failed in the splice performed very well with M_D/M_s ratios varying with the drop heights. Specimens IM-30T and IO-30T were not cycled over a sufficient number of loadings at the large drop heights used to produce a splice failure. Specimen CR1-30T did not fail in the splice after a total of 32 load applications (16 producing tension on the splice) with dynamic moments 10 to 20 percent greater than either M_s or M_y. Specimen C-30-1T was subjected to extremely large impacts which in one load cycle resulted in a total test moment of 66 percent above the static yield moment. Even with the high concrete strength

(f'_c = 3820 psi), the splice was not able to transfer the very large bar forces for many load applications. In Specimen C-30-2T the moments induced were as much as 33 percent above the static yield, and 20 cycles were required to produce a splice failure.

Reversed loading (excluding top bar splices) does not appear to be more severe than unidirectional loading. Specimens CR-1-30 (no stirrups) and CR1-30T (with stirrups) performed as well or better than similar unidirectionally loaded specimens (C-30-2 and C-30-2T). Specimen CR1-30T (f'_c = 3340 psi) never failed in the splice, while unidirectionally loaded Specimen C-30-2T (f'_c = 3820 psi) failed in the splice even though all three specimens had stirrups and the unidirectionally loaded specimens had higher concrete strengths.

The specimens with top bar splices (CR2-30 and CR2-30T) reflect the lower bond strength of the top bars. Specimen CR2-30T (with stirrups) failed in the top bar splice after 13 load applications while the companion beam CR1-30T which was subjected to similar loading, withstood 32 load cycles without splice failure. Specimen CR2-30 (no stirrups) carried dynamic moments of up to 10 to 20 percent above static or yield capacities, but only for several cycles of tension on the top bar splice. Specimen CR1-30 carried a total of 24 load cycles in which M_s and M_y were exceeded by about 10 to 20 percent.

The information from tests with 42 in. splices is limited. The failure of Specimen RS-42 was probably due to the relatively low concrete strength (f'_c = 2660 psi). Specimens IM-42 and IO-42 (f'_c = 3260 psi) exceeded the static yield moment without achieving a splice failure during the limited number of load applications made.

5.4 Influence of Rapid Loading Rates on Material Strengths

The observation of dynamic splice strengths well above the static strengths gave impetus to determining the effects of high strain rates on the properties of the reinforcing steel and the concrete. Therefore, it was necessary to obtain reasonably accurate rates of strain for both the steel and concrete from which estimates of the material strengths and resulting specimen strengths could be made.

Rate of Strain - Steel. Estimates of the rate of strain prior to yield were made to determine whether the observed yield stresses (which were higher than static yield) could be attributed to rate of strain. The rate of strain is influenced by the drop height and by the degree of beam cracking and deterioration present. The main problem in determining strain rates is the lack of a constant strain-time relationship in the initial portion of the curve up to yielding. For strain time curves such as shown in Fig. 5.1 initial constant slope may be reduced just prior to yield. In this case the dynamic yield stress would be less than under a constant high strain rate to yield. The rate for the initial straight region (ϵ_1) and the average rate over the entire elastic range (ϵ_2) are listed in Table 5.3 for the IO and IM series. The average yield strain (four readings) are listed and the yield stress is tabulated. The ranges include all gages showing yield during the load cycle considered. Dynamic yield strains (ϵ_{yD}) have been increased over the values in Table 4.1 to incorporate strains due to the dead weight of the beams (75, 120 and 170 μ in./in. for 18, 30 and 42 in. splices respectively) which were not included in Table 4.1. In Chapter 4 moments derived from strains were compared with moments obtained from reactions neither of which included the specimen weight. Differences between initial constant strain rates ϵ_1 and the average strain rates ϵ_2 are small. Strain rates were generally in the range 0.1 to 0.3 in./in./sec. The ratio of dynamic to static yield strain ranged from 1.16 to 1.29. Since the modulus of elasticity of the steel (29.2×10^6 psi) is not changed by strain rate the dynamic yield stress may have exceeded static yield stress by as much as 30 percent and may account for most of M_D/M_s ratios greater than one listed in Table 5.2.

The effect of high strain rates on the yield stress of Grade 60 reinforcing steel has been studied by Flathau [8] and is summarized in Fig. 5.2(a). Similar work has been done by Feldman, et al. [15] on reinforcing steel and is shown in Fig. 5.2(b). These studies indicate an increase in yield strength of 10 - 40 percent for strain rates from 0.1 to 0.3 in./in./sec, which is the range of strain rates measured in the impact tests. This is consistent with ratios of dynamic to static moment capacity observed.

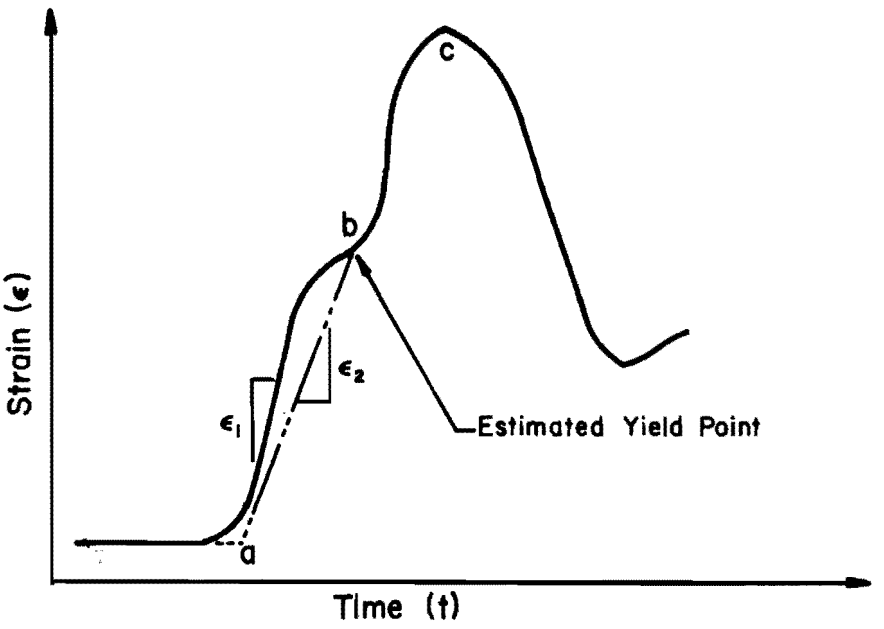

Fig. 5.1. Strain Rates - Steel

TABLE 5.3. DYNAMIC YIELD STRAINS AND STRAIN RATES

Specimen	Load Cycle	Average Dynamic Yield Strain, ϵ_{yD} μ in./in.	$\frac{\epsilon_{yD}}{\epsilon_{ys}}$*	ϵ_1 in./in./sec.	ϵ_2 in./in./sec.
IM-18	3	2510	1.16	0.18 - 0.20	0.15 - 0.18
IO-18	1	2510	1.16	0.27 - 0.42	0.19 - 0.29
IM-30	3	2660	1.23	0.16 - 0.23	0.11 - 0.21
IO-30	1	2790	1.29	0.21 - 0.29	0.19 - 0.28
IM-30T	3	2760	1.27	0.16 - 0.23	0.16 - 0.23
IO-30T	1	2650	1.22	0.20 - 0.31	0.20 - 0.31
IM-42	3	2560	1.18	0.15 - 0.25	0.13 - 0.20
IO-42	1	2790	1.29	0.19 - 0.21	0.19 - 0.24

*ϵ_{ys} = 2170 μ in./in.

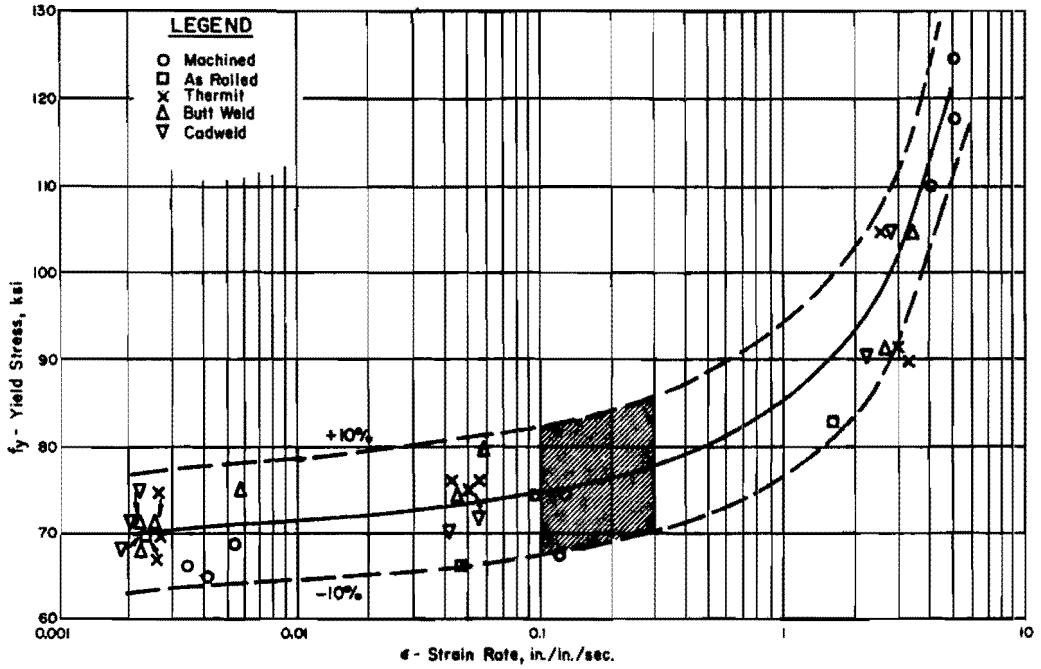

(a) Yield stress versus strain rate, Grade 60 bars.
(Flathau [8])

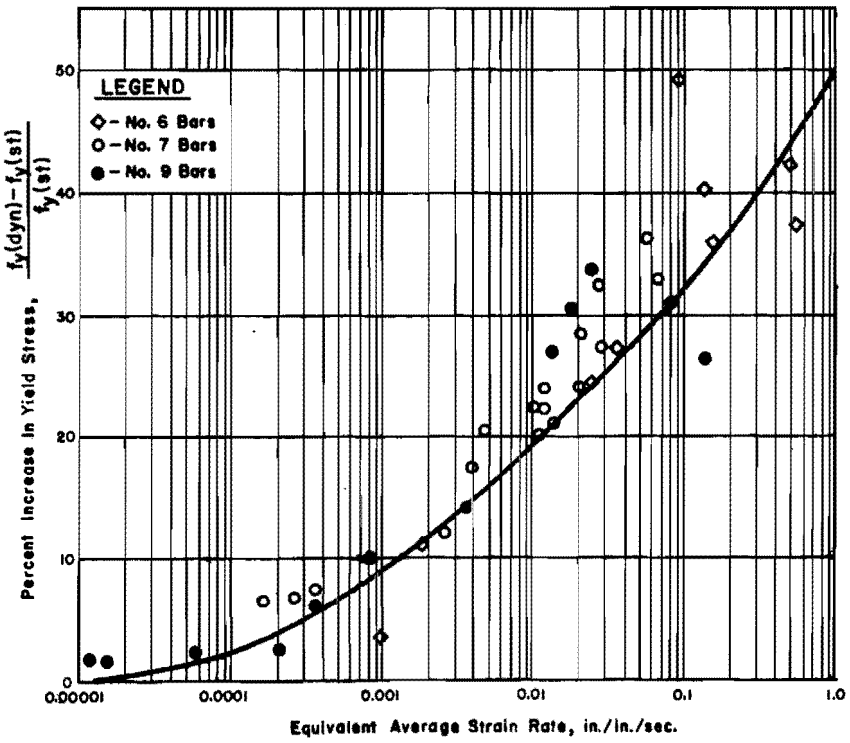

(b) Percent increase in yield stress vs average strain rate.
(Feldman, Keenan, Siess [15])

Fig. 5.2. Yield stress versus strain rate--reinforcing steel

Rate of Stress - Concrete. The concrete tensile splitting stresses which develop in the splice region must reflect the steel stress rates observed. However, the rate at which different sections along the splice are being stressed in tension cannot be determined, but estimates of the rates of the average splitting tensile stresses in the concrete can be made for the maximum loads and moments attained in a given load cycle. To do this, the maximum tensile strength of the concrete can be estimated. A stress rate can be based on the rise time taken to achieve maximum reactions and corresponding steel or concrete stresses. For instance, values of 6 to $7.5\sqrt{f'_c}$ (f'_c = ultimate concrete compressive stress in psi) are used to represent the static tensile strength of concrete. For a 4000 psi concrete, the maximum tensile capapacity is 470 psi. In the impact tests rise time of 15 to 25 ms. was observed. Dividing the tensile strength by an average rise time of 20 ms. (0.02 sec.), a stress rate of about 24,000 psi/sec. is obtained.

Galloway and Raithby [9] studied the effect of high stress rates (comparable to the ones used in the current investigation) on the modulus of rupture of plain concrete. The modulus of rupture can be assumed a reasonable indicator of the tensile splitting resistance of the concrete. The variation of the modulus of rupture with different stress rates was obtained for two concretes labeled PQ1 (uncrushed flint gravel aggregate) and PQ2 (crushed limestone aggregate). Both were designed to have the same indirect-tensile (split cylinder) strength after 28 days. Unit conversions are based on 1 MN/m^2 = million Newtons/$meter^2$ = 145.03 psi.

Indirect-tensile strength tests on 152 mm x 102 mm diameter (6 × 4 in. diameter) cylinders showed 28 day strengths of about 3.5 MN/m^2 (505 psi) for both PQ1 and PQ2 specimens. Compression strengths for 28 day 102 mm (4 in.) cubes were 44.80 MN/m^2 (6497 psi) and 33.30 MN/m^2 (4829 psi) for PQ1 and PQ2 specimens. Modulus of rupture results were obtained using 508 mm × 102 mm × 102 mm (20 in. × 4 in. x 4 in.) plain concrete beams loaded at the third points. The beams were water cured for 26 weeks prior to testing. Results are listed in Table 5.4.

TABLE 5.4. VARIATION IN MODULUS OF RUPTURE OF CONCRETE WITH STRESS RATE FROM REF. [6]

Concrete Type	Rate of Increase of Extreme Fiber Stress		Number of Tests	Mean Modulus of Rupture		% Increase With Respect to Slowest Rate
	MN/m^2/sec.	psi/sec.		MN/m^2	psi	
PQ1	0.0172	2.49	10	4.21	611	0
	0.172	24.9	11	4.64	673	10.1
	0.86	125.0	11	5.19	753	23.2
	1.72	249.0	12	5.17	750	22.7
	17.2	2495.0	10	5.86	850	29.1
	68.9	9993.0	10	6.32	917	50.1
	172.0	24950.0	10	6.97	1011	65.5
PQ2	0.0172	2.49	10	5.67	822	0
	1.72	249.0	5	6.54	948	15.3
	68.9	9993.0	5	7.66	1111	35.2

For concrete PQ1, a stress rate of 25000 psi/sec. produces an increase of 65 percent in the modulus of rupture over that observed using a very slow rate. The above stress rate is comparable to the 24000 psi/sec. estimated for the impact tests. Note that the increase in capacity is 50 percent for PQ1 and 35 percent for PQ2 for a stress rate of 10000 psi/sec. Therefore, it is likely that the concrete tensile strength increased sufficiently to permit dynamic yield stresses to be developed in the steel.

5.5 Toughness and Durability of Splices

The maximum splice capacity (moment) of a dynamically loaded beam is a very unsatisfactory strength parameter if a splice failure occurs several milliseconds after this moment is attained. Some ductility, toughness or durability must be available to prevent a brittle potentially catastrophic failure. To study this aspect of splice behavior under dynamic loading an attempt was made to describe the deterioration occurring with successive load applications and to define parameters which might measure durability features.

The inadequacy of maximum splice moment as a measure of dynamic performance can be seen in Table 5.2. For specimens with 18 in. splices, dynamic moments of around 1.70 times the expected static moment (based on static splice strength) could be carried for one or two large impact load cycles (Specimens IM-18, IO-18). By decreasing the mass drop height, more cycles of loading could be sustained prior to splice failure. With a 24 in. drop height, 3 cycles of loading (moments at 1.24 to 1.41 times the static moment) achieved splice failure. For a 16 in. drop height, 4 cycles with moment ratios of 1.11 to 1.35 were carried before the splice failed. For drop heights between 8 and 12 in., 10 load cycles producing splice moments of 1.01 to 1.33 times the expected static moment finally failed the splice. Specimens with 30 in. splices showed a similar pattern. The satisfactory performance of a splice is influenced not only by the moment magnitudes carried, but also by the duration of time over which the moments are sustained (measured indirectly by the number of load cycles in the above illustration).

Deflections. The increase in the residual deflection occurring with consecutive load applications was used as one parameter in describing the ductility of the splice beams. The ability to carry a high load level, even after considerable permanent deformation due to bar yielding or other inelastic behavior has taken place, ensures that the beam has some toughness or energy absorbing capability. Residual deflections provide a toughness measure for specimens always loaded from the same direction. For reversed loading, residual deflections do not tend to build up, since each following load application counteracts the residual deflection of the previous load cycle. Several deflections - number of cycles curves are shown in Figs. 5.3 and 5.4 and are typical of the impact tests. The residual deflection is cumulative from first loading.

The increase in maximum dynamic deflections occurring under consecutive load applications with equal energy levels provides a measure of the reduced stiffness and deterioration occurring in the beam for either unidirectional or reversed loading tests. Disproportionately large increases in either residual deflections or maximum deflections indicate impending splice failure.

In general, when dynamic moments are well over the static capacity, residual deflections build up more rapidly and peak cycle deflections are larger. Reversed loading residual deflections do not build up as rapidly as those under unidirectional loading.

Careful examination of the deflection data for specimens with 30 in. splices reveals that the single most important parameter in describing splice failure is the magnitude of the total (residual plus peak cycle) deflection occurring in the load cycle just prior to failure. These magnitudes are summarized in Table 5.5. For specimens without stirrups along the splice, the total deflection in the cycle prior to failure ranged from 0.85 in. to 1.33 in. With stirrups along the splice, the total deflection varied from 2.11 in. to 2.39 in.

The relative toughness or ductility of specimens with or without stirrups is related to the deflection that can be sustained before failure occurs. For specimens with 30 in. splices under impact loading, those

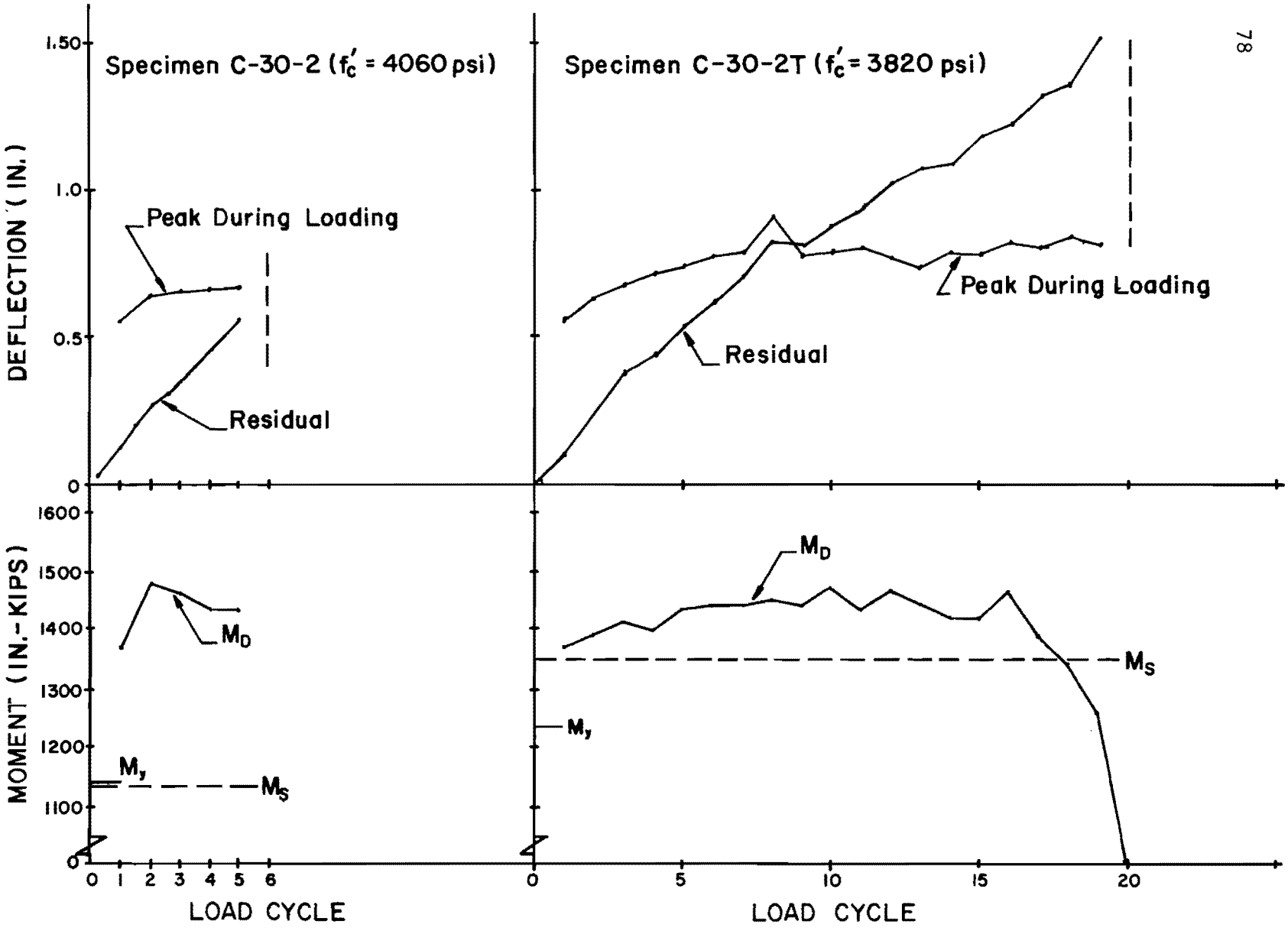

Fig. 5.3. Deflections at load points - unidirectional loading

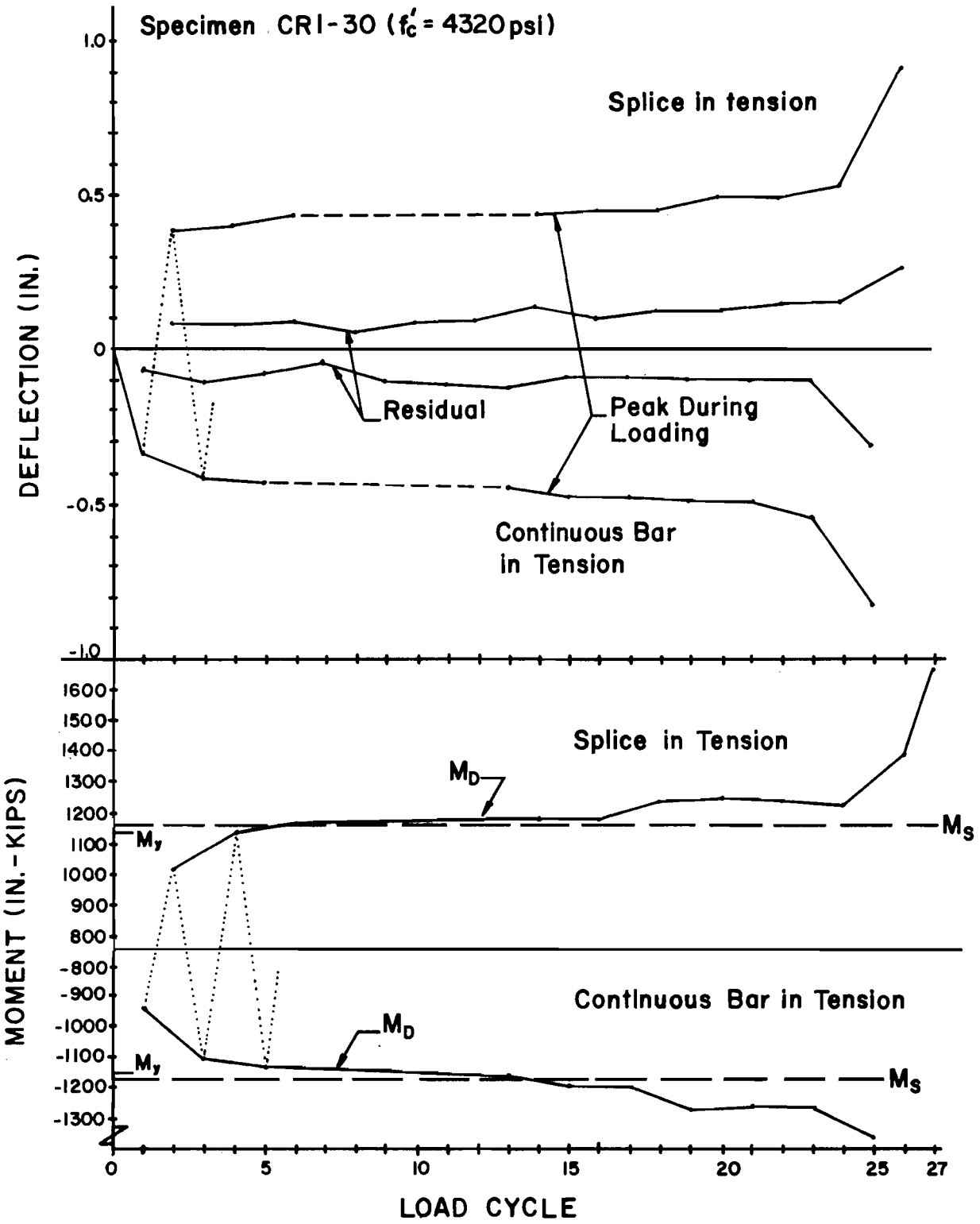

Fig. 5.4 Deflections at load points - reversal loading

TABLE 5.5. DEFLECTIONS OCCURRING PRIOR TO SPLICE FAILURE

Specimen	Cycle No.	Peak Deflection in.	Residual Deflection in.	Total Deflection in.
IM-30	3	0.71	0.14	0.85
C-30-1	2	1.24	0.09	1.33
C-30-2	5	0.69	0.52	1.21
IM-30T	6	1.28	1.11	2.39*
C-30-1T	3	1.12	0.99	2.11
C-30-2T	19	0.81	1.36	2.17
CR1-30	26	0.90	0.14	1.04
CR2-30	7	0.83	0.19	1.02
CR1-30T	32	1.12	0.06	1.18*
CR2-30T	12	1.09	0.32	1.41

*Specimen did not fail.

with splice stirrups sustain loading until a total deflection of over 2 in. is achieved, while specimens without stirrups fail in the splice at a total deflection of around .1 in. The behavior of Specimen S1-30Cb is consistent in that the total deflection (tension on splice) before the test was terminated was only 1.18 in. and would not be expected to produce failure for a specimen with stirrups.

Free Vibration of the Test Beam During Rebound Strain measurements provide data for indirectly determining the gradually deteriorating beam stiffness occurring with load cycling. The approach is to measure the time interval of the natural (free) vibration period of the beam specimen in an unsupported state. After application of the dynamic loading, the beam specimen rebounds from the reaction supports and vibrates for periods of 50 to 150 ms which is equivalent to about three to five cycles of free vibration of the beam. This rapid vibration of the beam is picked up by the steel strain gages, allowing the frequency or period of these

cycles to be easily measured. Increases in the periods with number of cycles of loading indicates a decreasing beam stiffness produced by deterioration of the beam or the splice.

Two strain-time traces are reproduced in Fig. 5.5. The figure clearly shows the regular vibrations occurring. Both traces in Fig. 5.5 are for the same gage in the same load cycle for the specimen considered. One was recorded using an effective tape speed of 64 in./sec. while the other was recorded at a speed of 4 in./sec. Because the vibration is measured at low levels of stress, amplitudes are of no concern. Therefore, many strain gages delivered useful information even after they were not suitable for measuring strain magnitude.

The increase in the natural vibration periods (free-free support conditions) with load cycling is shown in Fig. 5.6 for several specimens. Characteristics of the changing natural periods are very similar to deflection behavior. The period ranges are listed in Table 5.6. The maximum periods indirectly indicate the beam stiffnesses after impact provided splice failure does not occur.

The tabulated ranges (Table 5.6) for beam stiffnesses EI_{ave} are calculated assuming a prismatic beam. This permits the fundamental frequency or period to be related directly to beam properties using the following equation for free-free support conditions:

$$T = 2\pi\ell^2\sqrt{\frac{\mu}{500\,EI}} \quad \text{or} \quad EI = \left(\frac{2\pi}{T}\right)^2 \frac{\mu\ell^4}{500}$$

where T = fundamental natural period (from Table 5.6)

μ = unit length mass density = (wt./unit length)/g = $0.053 \frac{\text{lb.-sec.}^2}{\text{in.}^2}$
= weight per unit length ÷ acceleration of gravity

L = beam length (including overhangs)

EI = beam stiffness

The tabulated moments of inertia (I effective) are obtained by dividing EI_{ave} by the concrete modulus of elasticity ($E_c = 57000\sqrt{f'_c}$).

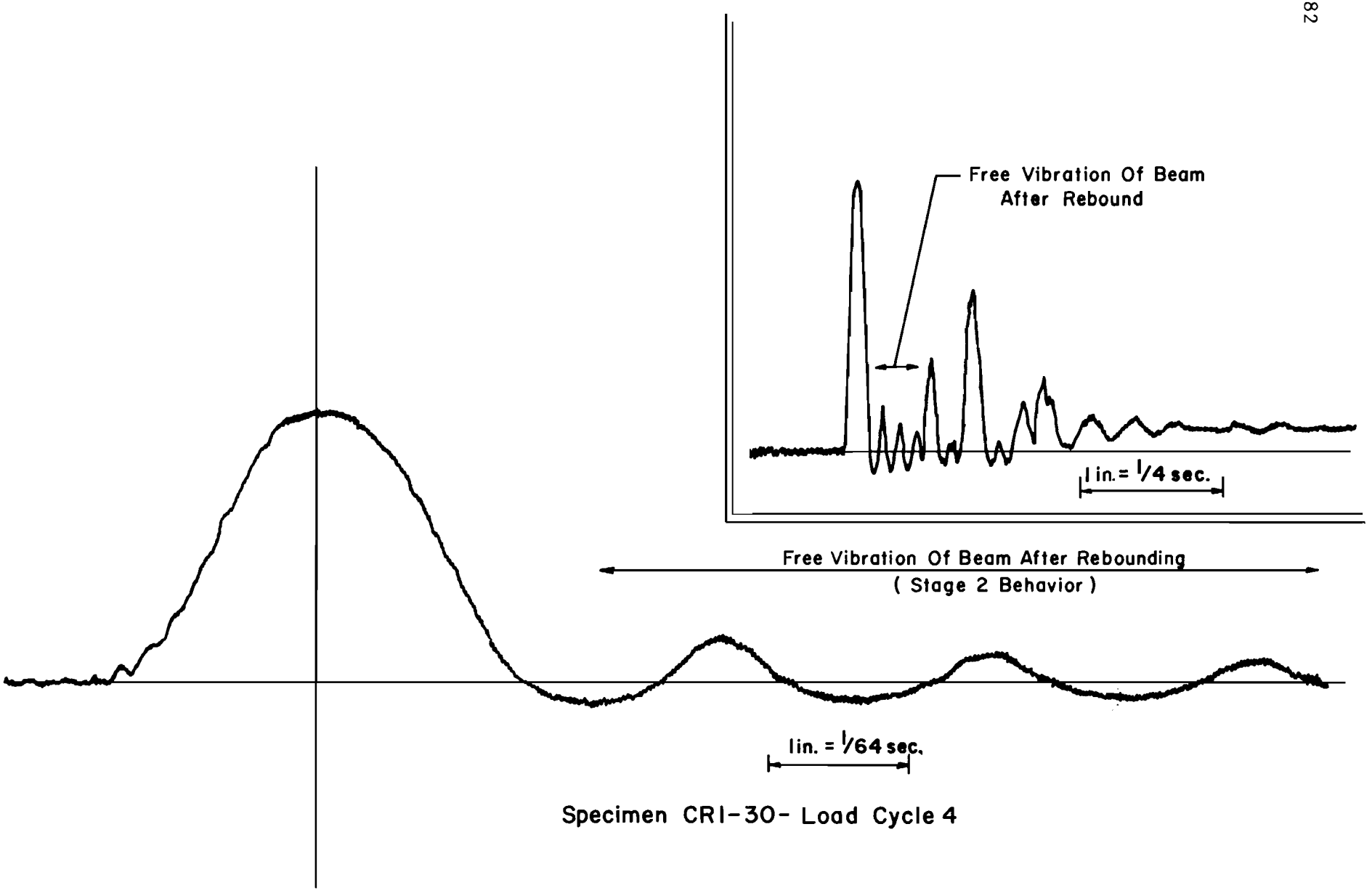

Fig. 5.5. Typical strain-time traces used in measuring the free vibration period of the specimens after rebounding.

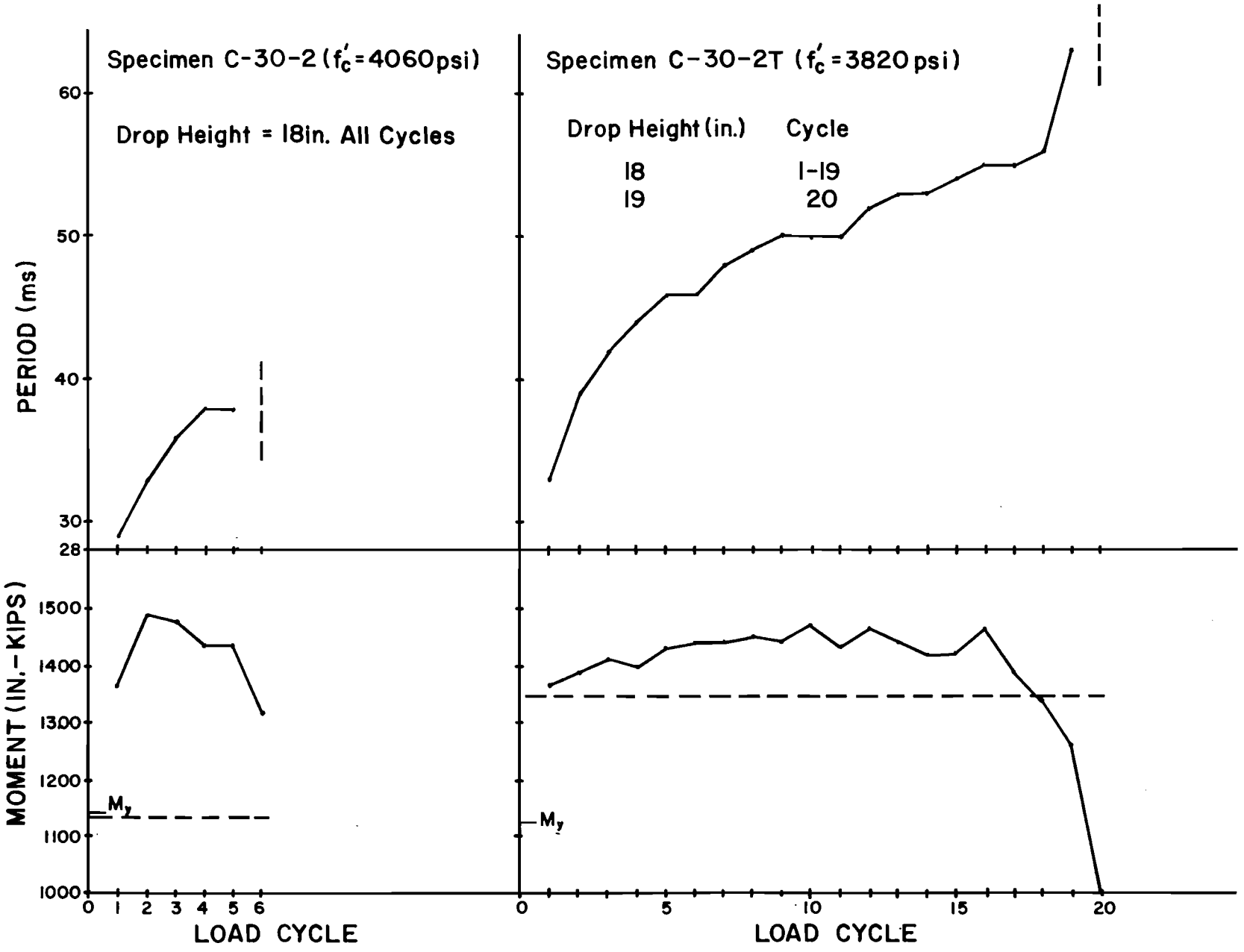

Fig. 5.6. Change in natural period with number of cycles.

TABLE 5.6. AVERAGE BEAM STIFFNESSES BASED ON FREE VIBRATION PERIODS

Specimen	Natural Period (T) ms	f'_c (psi)	E_c (psi x 10^6)	EI_{ave} (psi x 10^6)	I_{eff} ($in.^4$)
IM-18	15	3180	3.21	9160	2850
C-18-1	13 - 14	3330	3.29	12200 - 10500	3700 - 3190
C-18-2	12 - 29	3400	3.32	14300 - 2450	4310 - 745
C-18-3	13	3400	3.32	12200	3670
IM-30	21 - 33	3160	3.20	10300 - 4170	3220 - 1300
IM-30T*	18 - 38	3610	3.42	14000 - 3140	4090 - 920
IO-30T*	33	3610	3.42	4170	1220
C-30-1	19 - 31	4060	3.63	12600 - 4720	3470 - 1300
C-30-2	29 - 38	4060	3.63	5400 - 3140	1490 - 870
C-30-1T	27 - 63	3820	3.52	6230 - 1140	1770 - 320
C-30-2T	33 - 63	3820	3.52	4170 - 1140	1180 - 320
CR1-30	19 - 39	4320	3.75	12600 - 2980	3360 - 795
CR2-30	22 - 41	4320	3.75	9380 - 2700	2500 - 720
CR1-30T*	24 - 45	3340	3.29	7880 - 2240	2400 - 680
CR2-30T	24 - 45	3340	3.29	7880 - 2240	2400 - 680
IM-42*	31 - 45	3260	3.25	9160 - 4350	2820 - 1340
IO-42*	43	3260	3.25	4760	1460

*No splice failure at end of test.

I (gross section) $\approx 4800\ in.^4$
I (cracked transformed) $\approx 1400\ in.^4$

Stiffness after several cycles of impact loading was well below the cracked beam stiffness. Under similar conditions of reinforcing (stirrups or no stirrups) and loading (reversed or unidirectional), smaller drop heights eventually resulted in greater stiffness deterioration prior to failure.

Time Dependence. It is essential that the integrity of the splice remain intact over a number of load cycles of a desired load level, or stated in a different manner, the splice must carry a desired capacity over some minimum time interval. For a specimen subjected to a number of cycles of high intensity loadings, the usual definition of energy absorbing characteristics or toughness will not suffice.

Specimens in the C series were tested under loads having the same energy levels as measured by the mass drop height. The number of load cycles of constant drop height necessary to achieve failure thus gave a relative measure of the splice performance. For example, six load cycles were required to fail Specimen C-30-2 (no stirrups) while Specimen C-30-2T (with stirrups) required 20 load cycles at the same drop height. Many estimates of the energy absorbing capabilities of a beam could be made. The energy absorbed in all load cycles up to failure could be summed. Another method would be to estimate the energy absorbed by the vermiculite cushions and subtract it from the kinetic energy of the drop mass. However, energy is lost in many ways, such as, concrete cracking, rebound of the beam from the reaction supports and yielding of the steel bars. Energy lost in this manner has little influence on the splice performance. Another approach to evaluate dynamic splice capacity was based on determining the impulse carried by the splice at loads in excess of the static strength. Loading below static strength can be maintained indefinitely and was not considered in the impulse calculations. Average steel bar forces in the splice region were determined from the reactions to give bar force versus time responses as shown in Fig. 5.7. The force-time areas or impulses above the estimated static strength (shown shaded in Fig. 5.7) were determined. The static strength was calculated using the RS series and correcting to account for the differences in concrete strengths. No

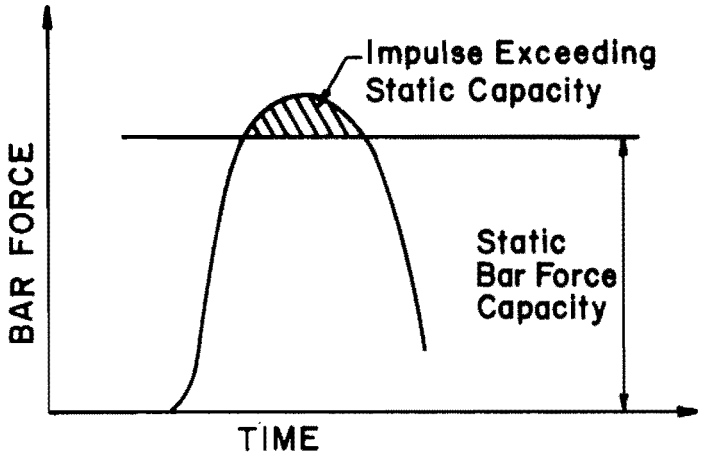

Fig. 5.7. Impulse measurement for dynamic capacity of splice beams

TABLE 5.7. IMPULSE CARRIED BY SPLICE IN EXCESS OF THE STATIC CAPACITY

Specimen	Impulse Over Static Capacity (kip-ms)	Col. ÷ (L_s Xb) (kip-ms.in.^{2})	Cycles @ Drop Height (in.)
IM-18	1080	3.5	1@10, 1@24, 1@28, 1@48
IO-18	610	2.0	1@45
C-18-1	700	2.3	3@24
C-18-2	1420	4.6	1@12, 2@10, 8@8
C-18-3	550	1.8	4@16
IM-30	1050	2.1	1@10, 1@24, 1@24, 1@40
IO-30	500	1.0	1@45
C-30-1	1340	2.6	1@10, 2@60
C-30-2	2040	4.0	6@18
C-30-1T	1320	2.6	1@14, 3@72, 1@84
C-30-2T	1420	2.8	20@18
CR1-30	1110+	2.2**	7@ 8, 2@ 9, 3@10, 1@24, 1@84
CR2-30	700+	1.4**	4@18
	530+	1.1**	4@18
CR2-30T	460+	0.9**	4@18, 1@21, 1@24
	270*	0.5	4@18, 1@21, 2@24

+Bottom bars.

*Top bars.

**No splice failure on this face.

clear trend was evident in any of the tabulations (Table 5.7). In general, higher total impulses (above static cpapcity) were carried when a specimen was impacted with smaller loadings and failure did not occur for many load cycles. It is evident that while very short splices may carry stresses at or near yield, the length of time over which these stresses can be maintained may be very short and have no practical significance.

CHAPTER 6

SUMMARY AND DESIGN IMPLICATIONS

For dynamic loads with strain rates as investigated herein, moments acting on the splice with magnitudes equal to the static capacity can be carried over many applications of unidirectional or reversed impact loading without deterioration leading to failure. When dynamic moments exceeding the static moment capacity are applied, the maximum splice capacity is dependent on the rate of loading. The loading rate establishes the dynamic yield stress of the steel and the dynamic tensile strength of the concrete. Either the concrete or the steel can limit the dynamic moment carried by the splice.

Evaluation of dynamic splice performance where the splice is loaded above the static capacity must consider toughness and durability characteristics. Parameters influencing the toughness and durability evaluations include the type of loading (unidirectional versus reversal, and large impact versus small impact), and the presence of stirrups along the splice.

Specimens were able to carry many cycles of loading prior to a splice failure if small drop heights were used so that moments did not significantly exceed the static moment capacity (say 5 to 10 percent over static moment). With very large drop heights, the dynamic moments were 40 to 50 percent (30 in. splices) or 70 to 75 percent (18 in. splices) above the static capacity, but splice failure resulted after very few cycles of loading.

Reversed loading appeared to be no worse than unidirectional loading. For similar specimens, smaller reactions and splice moments were induced for reversed loading with the same drop height because energy was absorbed in overcoming the inelastic residual deformation.

As expected, the placement of stirrups along the splice greatly enhanced all toughness and durability characteristics of the splice.

Dynamic loads were sustained with total deflections of at least twice the deflections found in similar specimens without splice stirrups.

In general, the dynamic moment capacity of a splice is at least as large and usually larger than the static moment capacity. Dynamic splice moments as large as the static capacity were safely carried for loading rates that induced steel strain rates as high as 0.3 in./in./sec. Therefore, a splice length based on design specifications developed using static test results would appear to provide adequate capacity under dynamic loading conditions provided shear was minimal in the splice region.

REFERENCES

1. Lew, H. S., Leyendecker, E. V., and Dikkers, R. D., "Engineering Aspects of the 1971 San Fernando Earthquake," U.S. Department of Commerce, National Bureau of Standards, Building Science Series 40, December 1971.

2. Bufkin, M. P., "Behavior of Concrete Reinforcing Bar Lapped Splices Subjected to Dynamic Loading," thesis for Master of Science in Engineering, The University of Texas at Austin, January 1974.

3. Ferguson, P. M., and Breen, J. E., "Lapped Splices for High Strength Reinforcing Bars," Journal of the American Concrete Institute, Vol. 62, No. 9 (September 1965), pp. 1063-1076.

4. Smith, E. F., and Thompson, J. N., "A Study of Vermiculite Concrete as Shock-Isolating Material," The University of Texas Structural Mechanics Research Laboratory, Austin, Texas, October 1963.

5. Nikkhah, M., Burns, N. H., and Thompson, J. N., "A Study of the Interaction of Cushioning Materials and Structural Elements," The University of Texas Structural Mechanics Research Laboratory, Austin, Texas, July 1965.

6. Ferguson, P. M., and Krishnaswamy, C. N., "Tensile Lap Splices, Part 2: Design Recommendations for Retaining Wall Splices and Large Bar Splices," Research Report 113-3, Center for Highway Research, The University of Texas at Austin, April 1971.

7. ACI Committee 318, "ACI Standard Building Code Requirements for Reinforced Concrete (ACI 318-71)," American Concrete Institute, Detroit, Michigan, November 1971.

8. Flathau, W. J., "Dynamic Tests of Large Reinforcing Bar Splices," Technical Report N-71-2, U.S. Army Engineer Division, Huntsville, Alabama, April 1971.

9. Galloway, J. W., and Raithby, K. D., "Effects of Rate of Loading on Flexural Strength and Fatigue Performance of Concrete," Transport and Road Research Laboratory, Department of the Environment, TRRL Report LR547, Crowthorne, Berkshire, 1973.

10. Tepfers, R., "A Theory of Bond Applied to Overlapped Tensile Reinforcement Splices for Deformed Bars," Publication 73:2, Division of Concrete Structures, Chalmers University of Technology, Göteborg, Sweden, 1973.

11. American Association of State Highway and Transportation Officials, Interim Specifications - Bridges, 1974.

12. Rezansoff, T., "Performance of Lapped Splices under Rapid Loading," Ph.D. dissertation, The University of Texas at Austin, 1975.

13. Orangun, C. O., Jirsa, J. O., and Breen, J. E., "The Strength of Anchored Bars: A Reevaluation of Test Data on Development Lengths and Splices," Research Report No. 154-3F, Center for Highway Research, The University of Texas at Austin, 1975.

14. Thompson, M. A., Jirsa, J. O., Breen, J. E., and Meinheit, D. F., "The Behavior of Multiple Lap Splices in Wide Sections," Research Report No. 154-1, Center for Highway Research, The University of Texas at Austin, 1975.